OSLO METROPOLITAN UNIVERSITY
STORBYUNIVERSITETET

Department of Civil Engineering and Energy Technology
Institutt for Bygg- og energiteknikk
Energi og miljø i bygg
Postadresse: Postboks 4 St. Olavs plass, 0130 Oslo
Besøksadresse: Pilestredet 35, Oslo

Telefon 67 23 50 00
www.oslomet.no

Oppgave/kandidat nr.
406

Tilgjengelighet
Open

MASTER'S THESIS

Masteroppgavens tittel	Dato
A detailed analysis of transient flow through doorways using CFD	2022-05-24
	Antall sider/antall vedlegg: 69/5
Forfatter: Fredrik Kihlberg	Veileder: Arnab Chaudhuri

Utført i samarbeid med	Kontaktperson

Sammendrag
The quality of our indoor environment influences our mental and physical health. Fluid flow is a factor that influences this, which can be analysed using computational fluid dynamics (CFD) software. In this thesis the finite volume method (FVM) based software Star-CCM+ was used to model different type of doors separating two zones, one containing a tracer gas mixture and the other containing air. The Reynold-averaged Navier Stokes (RANS) equations were used with a $k-\epsilon$ turbulence model to solve for 3D compressible multi-component fluid flow, with an overset mesh being used for moving solids. For both the verification model and the case model, a comparative analysis considering cumulative mass exchange was performed. For the case model, thermal effects and human motion were also included.

3 stikkord
CFD
Door motion
Indoor air flow

Preface

This masters thesis represents the end of the degree "Energi og miljø i bygg – sivilingeniør" at Oslo Metropolitan University - Storbyuniversitet. The work for this thesis has been done in the spring of 2022.

First of all, I would like to thank my supervisor Arnab Chaudhuri! I deeply enjoyed your course on fluid mechanics and CFD. Your passion for your field really shines through. You always dealt with all my simulation errors, moments of stress, and panic-laced emails in a calm and helpful manner. You have my eternal gratitude, and I wish you only the best. I would also like to thank professor Sergiy Denysov, whose course on differential equations calculus helped me appreciate, and maybe even understand, the math behind fluid mechanics a little better.

I would also like to thank my parents and my siblings, for being there for me when I needed to either vent my frustration, or just take my mind off everything school-related for a few minutes. A big thank you to Greta, Charlene and Alex for proofreading drafts, and for just being wonderful people! A thank you to UiT - Arctic University of Norway for granting my department access to their super-computer cluster Fram (under the project NN8005K at Notur, UNINETT Sigma2 AS (National infrastructure for scientific computational science in Norway)). Without this access I'm pretty sure I'd still be running simulations.

The biggest thank you goes to my girlfriend Anna and our son Brage. You have both been the shining beacon of light and love that got me through these past five years. Thank you for keeping me grounded, and for reminding me that sometimes the most important thing you can do is put the books down and go outside and play tag for a while. You are the joy of my life. I love you more than I can put into words!

On that rather sentimental note, I have always been a very curious person, and with this degree complete I find myself with so many new topics to be curious about! This trait along with this thesis, and all the courses and work leading up to it, has made me confident in my capability as an engineer. Thank you to Oslo Metropolitan University for having me these past five years!

Summary

The quality of the indoor environment directly influences our physical and mental health. With more and more time being spent indoor, it is becoming increasingly important to understand how fluids flow throughout a building. Fluid mechanics is an area of physics which defines the motion of fluid, and is used in many areas of engineering. Computational fluid dynamics (CFD) is a branch of this field where powerful hardware is used to solve complex fluid flow simulations.

In this thesis a finite volume method (FVM) based CFD software was used, where the RANS-equations with $k-\epsilon$ turbulence model was used to solve 3D compressible multi-component fluid flow, utilizing an overset mesh strategy to deal with the rigid body motion of both different type of doors and a model human being. Two domains were defined, one containing a tracer gas mixture and the other air. A flow field was defined in the doorway separating the two domains where transient flow data was collected and used for post-processing.

To verify the software being used a verification model was considered. All three door types used in the case model were also simulated here. This model was smaller in scale, and did not consider thermal effects or the rigid motion of a model person. A comparative analysis considering the cumulative mass exchange through the doorway was performed for each type of door. The results obtained from these matched with what previous numerical experiments have shown. The case models in this thesis advanced the work done in the verification model by introducing human motion and a temperature difference between the two domains, with a bigger computational domain.

The preliminary results obtained from the simulations showed that the mass flux of SF_6 was greatest with the hinged door. Previous studies have also showed that this type of door is associated with greatest mass transfer. The thermal analysis showed that the sliding door was responsible for transferring the most energy *into* the inner domain while the double sliding door transferred the most energy *out from* the inner domain.

In conclusion, Star-CCM+ has proven to be a powerful tool. Simulating moving solids with an overset mesh is a valid approach when doing these kinds of numerical experiments. The computational power and time required to run these simulations is a limiting factor that should always be considered. The simulations run in this thesis are of special interest in hospital and cold storage settings.

Sammendrag

Vår fysiske og mentale helse påvirkes direkte av kvaliteten av miljøet innendørs. Vi bruker mer og mer tid innendørs, derfor har det blitt meget viktig å forstå hvordan væsker beveger seg gjennom en bygning. Strømningsteknikk er et område innen fysikk som definerer bevegelsen til væsker, og brukes innenfor mange ingeniør-felt. CFD er et felt innen dette området hvor kraftig maskinvare blir brukt til å løse komplekse strømningssimulasjoner.

I denne avhandligen blir en FVM basert CFD programvare brukt, hvor RANS-ligningene blir brukt sammen med $k - \epsilon$ turbulens modellen for å løse for 3D komprimerbar multi-komponent strømning, ved bruk av en overordnet mesh strategi for å takle beveglesen av stive legmer - ulike typer dører og en modell av et menneske. To domener ble definert med den ene som inneholder en sporingsgass mikstur og den andre som inneholder luft. Et strømningsområde ble definert i døråpningen hvor ikke-stasjonære data ble samlet inn og ble brukt for etterbehandling.

For å verifisere programvaren brukt ble en verifikasjonsmodell designet. Alle tre typer dører brukt i modellen ble også simulert her. Denne modellen hadde mindre dimensjoner, og tok ikke hensyn til termiske effekter eller menneskelig bevegelse. En komparativ analyse som vurderte den kumulative massen utvekslet gjennom døråpningen ble gjenomført for hver type dør. Resultatene fram disse simuleringene stemmer overens med det tidligere forskning har vist. Modellen i denne avhandlingen videreför arbeidet gjort i verifikasjonsmodellen ved å introdusere menneskelig bevegelse samt en temperatur differanse mellom de to domenene. Dimensjonene i denne modellen ble også økt.

De foreløpige resultatene fra disse simuleringene viser at masse fluksen til SF_6 var størst med hengslet dør. Tidligere studier har vist at denne typen dør er assosiert med størst masse overføring. Den termiske analysen viste at skyvedøren overførte mest energi *in til* det indre domenet, mens dobbel skyvedøren overførte mest energy *ut av* det indre domenet.

Det kan konluderes med at Star-CCM+ er et kraftig verktøy. Det å simulere bevegende solider med et overordnet mesh er en gyldig tilnærmning når slike numeriske eksperiment skal gjøres. Kraften og tiden som kreves av maskinvaren er en begrensende faktor og bør alltid overveies. Simuleringene fremført i denne avhandligen er av spesiell interesse for både sykehus og kjølelager.

Contents

1 Introduction

1.1 Background

In modern society a lot of time is being spent indoors. The quality of the indoor climate directly affects our health and cognitive abilities. As such, it is vitally important that we make sure the indoor climate is as good as possible. In order to ensure the quality of this climate, we need a firm understanding of fluid mechanics. Fluid mechanics is an area of physics which explains the motion of fluids, and is a steady companion in many fields of engineering. Understanding the behaviour of fluids, whether they flow through ducts or pipes, or through open spaces is key when designing the layout of technical installations.

In general, it is important to analyse fluid flow across zones for a variety of reasons. In office or residential areas these types of analyses could help reduce the risk of draft, reduce the heating or cooling load of a zone, and also help reduce the risk of airborne contaminants infecting users of the building. This last point has become very important ever since the COVID19 pandemic. These analyses could also help when planning the layout and door placement in a zone. Different parts of a building could have very different needs when it comes to airflow; a walk-in freezer will have very strict demands while a supply cupboard will not.

There are also more specialized rooms where the air quality and flux between zones needs special attention. In hospitals there are many different types of rooms which require special attention. Isolation and quarantine rooms have very strict guidelines for how they should interact with their surrounding areas. Medical laboratories and surgery rooms demand very clean air to avoid infections and contamination. This is of course true for most laboratories, although the type of contaminant may differ. In a microelectronics laboratory one might be more focused on keeping dust particles out than in a biology laboratory. Another field which requires strict cross-zone flux control is the nuclear industry. The dangers of radioactivity are well known, and limiting the radioactive particles to areas where they can do little to no harm to humans and nature is vital.

Considering cold room storage, it becomes important to know the effect of heat transfer when opening and closing doors into the zone. Unwanted heat transferred into the room can have a significant impact on the energy demand of the cooling system. A rise in temperature inside the room could also reduce the quality or downright spoil the stored materials, such as foodstuff or biological or chemical samples.

1.2 Literature review

Opening and closing of doors lead to air volume exchange between zones, see figure 1 for an example of vorticity generated by the motion of a door. Tian et al. [1] investigated the air flow created by opening and closing a hinged door. To help visualize the results they used a tracer gas. Their findings showed that opening and closing a door creates vortex motion around the surfaces of the door, with closing the door generating the largest vortexes. Chang et al. [2] did a CFD simulation of a control room examining air leakage into the room when doors are opening and closing. They showed that during door closing leakage was pushed by the front face and flowed round the door edges to the back face. Fontana and Quintino [3] did a small scale model and an experimental model of adjacent rooms. Their models used hinged type doors. They showed that door motion can lead to contaminated clean rooms. Hendiger et al. [4] did a scale

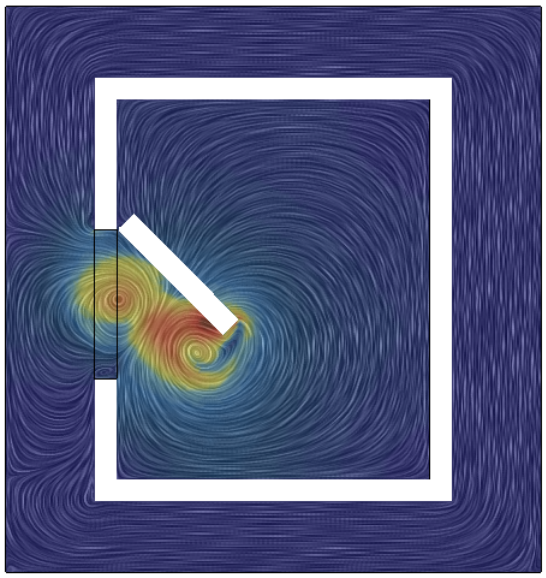

Figure 1: Vortex generation around a moving door

model of two connected rooms. They used smoke as tracer fluid. They tested opening doors both towards positively and negatively pressurized zones. Their findings showed that quickly opening doors causes greater transfer of tracer fluid. They also showed less fluid transfer when opening door towards negatively pressurized zone. Shao et al. [5] did an experimental analysis of a clean room with double hinged doors. They used a particle generator to simulate transmission. They showed that personnel walking past the open door instantaneously increased transmission. Their findings also showed that transmission reduced when the airflow through the doorway increased.

In addition to the general studies there have also been numerous studies examining more specialized cases like the effect door motion has on cold storage facilities. Ayarmal et al. [6] showed that the presence of an active fan in a cold storage room increases the air exchange volume as well as the air mixing pattern. They reasoned that this could indicate that for rooms with active fans, door motion and fan control becomes important in order to reduce the cooling load, as well as prevent unwanted air mixing. Gonçalves et al. [7] and Wang et al. [8] performed numerical analyses of air volume and temperature exchange between a cold storage and a corridor. They showed that hot air enters the cold room in the top half of the doorway, and cold air leaves the cold room in the bottom half. They also showed that air velocity was greatest around the edges of the doorway. Tian et al. [9] did numerical modelling of a cold storage room with a large number of mesh cells. They showed that a low temperature difference between the room and the corridor reduced air infiltration between the two zones. They also showed that the size of the door affected the infiltration rate. Zhang et al. [10] did a numerical study of refrigerated vehicles, examining the time taken for the temperature inside to equalize with the temperature outside. Their study showed that door placement influences the time taken for temperatures to equalize.

Cold storage analysis is more focused on the thermal effects, but hospital setting is most definitively more concerned with air flow patterns and mass transfer. Especially with the COVID19

pandemic it has become vitally important to understand the way fluids flow, and possibly carrying unwanted particles with them, across zones in buildings. Zhou et al. [11] did a CFD simulation examining fluid contamination between an operating room and its anteroom. They showed that contamination is reduced when the temperature of the operating room is greater than the temperature of the anteroom. They also showed that cross-zone contamination is significant when the door between the zones is fully opened, and when the door is closing, due to vortex generation. Kalliomäki et al. [12] did a physical model study of a hospital isolation room. They showed that the temperature difference as well as the air flow rate of the ventilation system influenced the air exchange volume between the zones. Mousavi et al. [13] examined door motion and door usage in a real hospital operation room. In their experiments the average door opening time was 4 seconds. They showed that personnel using the door to enter or exit the room spent more time than needed doing this. Bhattacharya et al. [14] did a full scale model of a chaser room and a clean room. They used tracer particles to measure traffic from the chaser room and into the clean room. Their results showed that door motion contributed to spread of particles. Hathway et al. [15] did a field and small scale study of rooms with hinged type doors in office and hospital settings. In their small scale model they used water as tracer fluid. They showed that there exists a linear relationship between the time doors are held open and air volume flux. Kalliomäki et al. [16] did a full scale model of a hospital isolation room using hinged and sliding doors. To measure air flow they used tracer gas. In addition to door motion they also moved a manikin through the door during its opening phase to simulate a person entering the room. They showed that the air change per hour was greater for the hinged type door. They also showed that with the manikin moving through the door the effect was more noticeable. Bhattacharya et al. [17] did a physical model study of a positively pressurized room. The goal of this study was to examine the possibility of the COVID19 virus contaminating clean areas due to door opening and closing motion. They showed that clean rooms with no source of contamination were at risk of being contaminated due to the movement of doors and people moving in and out of the room. This risk decreased when the pressure difference between zones increased.

To better understand cross-zone fluid flow one should also compare different type of doors. Lee et al. [18] looked into the air exchange volume for both hinged and sliding doors using CFD models. They showed that for isothermal cases hinged doors caused a greater air exchange volume. They also showed that for thermal cases the effects were more prominent for sliding doors, even though hinged doors still had a greater air exchange volume. Similarly, Carneiro et al. [19] utilized a CFD model to examine the temperature increase and air volume exchange between a corridor and a cold storage room when different types of doors were used. While the temperature increase were approximately the same for both types of doors used, the air volume exchange increased by 50% when hinged doors were used.

Tian et al. [20] suggests the use of an empirical model instead of a CFD model. They used tracer gas to track fluid motion. When comparing results with their experimental model they showed similarities with $\pm$ 10 % prediction error. This prediction error is much higher than in cases which used CFD models to validate their findings. This study also highlights the greater level of accuracy one can achieve by including CFD simulations in the experiment.

1.3 Human motion and mass transfer

In addition to fluid flow being generated by the opening and closing of doors, there is also the human motion factor to consider. People walking by and through doorways will influence the way fluid flows in the region, as well as being a possible contributor to heat and mass transfer.

Heat transfer through doorways is important to consider when analysing cold storage rooms. A shift in temperature can compromise the stored inventory, such as food or biological test-samples. It can also lead to an increased power demand of the in-room cooling unit(s). Mass transfer through doorways is an important factor for both laboratories and facilities which work with radioactive materials, such as nuclear power plants. Mass transfer in the form of dust particles is undesirable for laboratories which work with microelectronics, where even the smallest particle can cause components to malfunction. For biology and chemistry laboratories mass transfer in the form of small organisms is unwanted as this can lead to faulty reactions and compromised growth cultures.

1.4 Computational fluid dynamics

When performing fluid mechanics experiments, modern engineers tend to perform both an experimental and a computational fluid dynamics (CFD) analysis. There are many advantages from performing both of these analyses, different data can be extracted from each. The experimental model can also be used to validate the CFD model.

Modern CFD software can handle laminar flow with ease. However, most modern engineering projects require turbulence models to be solved. In addition to this there is no *one* turbulence model that covers all possible scenarios. Therefore it is very important that engineers working with CFD models fully understand the problem they wish to examine, as well as the underlying physics.

Star-CCM+ is a CFD software initially developed by CD-adapco and was later purchased by Siemens Digital Industries Software. It allows for modelling and analysis of fluid mechanics problems, as well as particulate flow, electromagnetic, stress, and heat transfer. This software requires powerful hardware, but is capable of running very large and complex simulations [21].

1.5 Audience

The intended audience of this thesis is anyone who would like to know more about CFD models, and how these can be used to analyse help explain indoor climate. This work is of special importance, however, for anyone working with cold storage, indoor climate in hospitals, and CFD engineers.

1.6 Aim and objective

The aim of this thesis is to gain a better understanding of indoor air flows associated with door motion by numerical approach using CFD techniques. This work will focus on the motion of humans and different type of doors, and how they influence fluid and heat flow between zones. For this purpose a systematic comparison of the three different doors, namely sliding, hinged, and double sliding will be performed. Apart from resolving detailed flow, transfer of heat and the mass of a tracer gas between two zones will be measured, as well as fluid velocity. This is important as it will help understand how different fluids interact with each other in these types of situations. If one imagines one of the fluids as being contaminated with some infectious disease this work becomes especially important when considering the COVID19 pandemic. To the authors knowledge there is sparse literature examining the effect double sliding doors has on air flow through doorways, so this thesis aims to add new findings to the existing knowledge.

1.7 Scope and limitations

This thesis is an advancement of the work done by Hermansen [22]. The scope of this thesis is to examine the effect door and human motion has on turbulent flow in a region. The biggest limitation of this thesis is the calculation time required to run CFD simulations. The more mesh points a model in Star-CCM+ has the longer it takes to run the simulation to completion. When using a home or school computer the computational power is often limited for these types of models, and when using more powerful hardware like supercomputers one does not have unlimited access.

In this section an introduction to the research field has been given. Section two explains the governing equations used in CFD, the method of designing a model in Star-CCM+, what software was used for post-processing, and the use of super-computer. Section three explains the setup of the verification models and compares the preliminary results obtained from the simulations. Section four details the setup of the case models used in this thesis, while section five presents the results obtained from the simulations and gives a comparative analysis. Section six concludes this thesis and offers possible future work.

2 Method

In this section the method used in this thesis is explained in detail. The first part explains the theory of the equations used in the CFD simulations. The second part specifically explains the RANS-equations, as well as turbulence modelling and near-wall treatment. Finally the software used, Star-CCM+ and MATLAB, and how simulation jobs were submitted to the supercomputer cluster are explained.

2.1 Governing equations

The governing equations come from the conservation laws of physics, and state that:

- The mass of a fluid is conserved
- The rate of change of momentum equals the sum of the forces on a fluid particle (from Newton's second law)
- The rate of change of energy is equal to the sum of the rate of heat addition to and the rate of work done on a fluid particle (from the first law of thermodynamics)

A fluid should also be considered as a continuum, that is a continuous, homogeneous matter with no holes. Note that the continuum assumption is an idealization of fluid flow. It is a valid assumption as long as the considered system is far larger than the space between molecules. The equations defined below are explained in greater detail in Versteeg [23].

The continuity equation describes the 3-dimensional unsteady flow of a compressible fluid:

$$\frac{\partial \rho}{\partial t} + \nabla \cdot (\rho u) = 0 \tag{1}$$

where ρ is the density of the fluid, u is the velocity within the fluid, and t is the time.

The momentum equation describes the momentum of the flow depending on the forces that are acting on the fluid and is defined as:

$$\frac{D(\rho u)}{Dt} = -\frac{\partial p}{\partial x} + \nabla \cdot (\mu \nabla u) + S_M \tag{2}$$

where p is pressure, μ is the dynamic viscosity and S_M is the source term.

The conservation of energy equation, when the first law of thermodynamics has been applied, can be written as:

$$\frac{D(\rho E)}{Dt} = -\rho \nabla \cdot u + \nabla \cdot (k \nabla T) + S_e + \Phi \tag{3}$$

where E is energy, k is the thermal conductivity of the fluid, T is the temperature, S_e is the energy source term, and Φ is the dissipation due to deformation work term.

The ideal-gas equation of state describes the relation between the pressure p, density ρ, the gas constant R, and temperature T. This equation describes a hypothetical substance but it can be applied to most common gases with a negligible percentage of error, usually less than 1% [24, Ch. 2]. The equation states that:

$$p = \rho R T \tag{4}$$

Equation 1, 2, and 3 above can be written in a general form called the transport equation. For any conserved property this can be written as:

$$\frac{D(\rho\varphi u)}{Dt} = \nabla \cdot (\Gamma \nabla \varphi) + S_\varphi \tag{5}$$

where φ is some scalar property and Γ is the diffusion coefficient. The governing equation defines advective terms on the left hand side and the diffusion and generation terms on the right hand side.

The governing equations can be rewritten into a more compact form called the material derivative or the advective derivative. This equation describes the time rate of change for some property φ and is defined as:

$$\frac{D(\rho\varphi u)}{Dt} = \frac{\partial(\rho\varphi)}{\partial t} + \nabla \cdot (\rho\varphi u) \tag{6}$$

This is a more compact way of writing the governing equations, which involves the transient term of the governing equation and the convective term. These are the equations CFD simulations solves, in general. For turbulent flow, the Reynolds averaged Navier-Stokes (RANS) equations can be used.

2.1.1 RANS-equations

There are many approaches to CFD simulations: Direct Numerical Simulation (DNS), Large Eddy Simulation (LES), Reynolds Averaged Navier–Stokes (RANS), and Coherent Vortex Simulation (CVS) to mention a few. For this thesis the RANS-equations will be used, and is explained further in this section.

The Navier-Stokes equation is one of the corner-stones of fluid mechanics. It describes the flow of viscous, Newtonian fluid. While the equation is not yet fully understood, it is a frequent tool used within physics and engineering. The Navier-Stokes equation is based on Newton's second law, which describes the relationship between the change in a particles' momentum and the resulting force. In cartesian coordinates the equation is applied to each fluid volume in the x-, y-, and z-directions. The first two parts of the equation describes the acceleration of the fluid and the last two parts describe the forces acting upon the fluid.

In 3-dimensional flow there are four unknowns to take into consideration: the velocity in the three directions - u, v, w - as well as the pressure p. The sum of the mean and fluctuating component of these unknowns can be defined as:

$$u = U + u' \tag{7}$$

$$v = V + v' \tag{8}$$

$$w = W + w' \tag{9}$$

$$p = P + p' \tag{10}$$

By taking the time average, continuity can be rewritten as:

$$\frac{\partial \bar{P}}{\partial t} + \nabla(\bar{p}\tilde{u}) = 0 \tag{11}$$

The Reynolds Averaged Navier-Stokes equations describe incompressible flow in 3 dimensions. In Cartesian coordinates, the velocity vector **u** has three components: x-component u, y-component v, and z-component w. The velocity vectors **v** and **w** has similar components.

$$\frac{\partial(\bar{p}\tilde{U})}{\partial t} + \nabla(\bar{p}\tilde{U}\tilde{u}) = -\frac{\partial \bar{P}}{\partial x} + \nabla(\mu\nabla\tilde{U}) + \left[-\frac{\partial\overline{(\bar{p}u'^2)}}{\partial x} - \frac{\partial\overline{(\bar{p}u'v')}}{\partial y} - \frac{\partial\overline{(\bar{p}u'w')}}{\partial z}\right] + S_{MX} \tag{12}$$

$$\frac{\partial(\bar{p}\tilde{V})}{\partial t} + \nabla(\bar{p}\tilde{V}\tilde{v}) = -\frac{\partial \bar{P}}{\partial y} + \nabla(\mu\nabla\tilde{V}) + \left[-\frac{\partial\overline{(\bar{p}u'v')}}{\partial x} - \frac{\partial\overline{(\bar{p}v'^2)}}{\partial y} - \frac{\partial\overline{(\bar{p}u'w')}}{\partial z}\right] + S_{MY} \tag{13}$$

$$\frac{\partial(\bar{p}\tilde{W})}{\partial t} + \nabla(\bar{p}\tilde{W}\tilde{w}) = -\frac{\partial \bar{P}}{\partial z} + \nabla(\mu\nabla\tilde{W}) + \left[-\frac{\partial\overline{(\bar{p}u'v')}}{\partial x} - \frac{\partial\overline{(\bar{p}u'v')}}{\partial y} - \frac{\partial\overline{(\bar{p}w'^2)}}{\partial z}\right] + S_{MZ} \tag{14}$$

The time-average scalar transport equation is defined as:

$$\frac{\partial(\bar{p}\tilde{\Phi})}{\partial t} + \nabla(\bar{p}\tilde{\Phi}\tilde{U}) = \nabla(\Gamma_\Phi\nabla\tilde{\Phi})\left[-\frac{\partial\overline{(\bar{p}u'\varphi')}}{\partial x} - \frac{\partial\overline{(\bar{p}v'\varphi')}}{\partial y} - \frac{\partial\overline{(\bar{p}w'\varphi')}}{\partial z}\right] + S_\Phi \tag{15}$$

In equations 11-15 the overbar indicates a time-averaged variable and the tilde indicates a density weighted variable.

2.1.2 Turbulence model

To paraphrase professor Sergiy Denysov at OsloMet University:

> *"In textbooks equations are nice and neat. In real life equations are ugly and complicated. Then again, such is life."*

This rings especially true when dealing with turbulence. Turbulent flow is characterized by chaotic and unpredictable flow. The flow characteristics is defined by its Reynolds number, which is give by:

$$Re = \frac{uL}{\nu} \tag{16}$$

where u is the fluid velocity, L is the characteristic length, and ν is the kinematic viscosity. See figure 2 for an example of flow moving from laminar to turbulent flow.

When dealing with laminar flow, several simplifications can be made to the RANS equations which allows for analytical solutions. Most flow encountered in fluid mechanics engineering however is turbulent. Turbulent flow offers no analytical solutions. Therefore, turbulence models are needed to solve the RANS equations. One can of course try to solve these equations by hand and while there can be joy to be found in doing large, complicated equations by hand, completing them in a reasonable time frame and remain confident that the results are accurate is a bit like trying to cut down a mighty tree using a herring: impossible. Solving turbulence models is therefore best left to computer software.

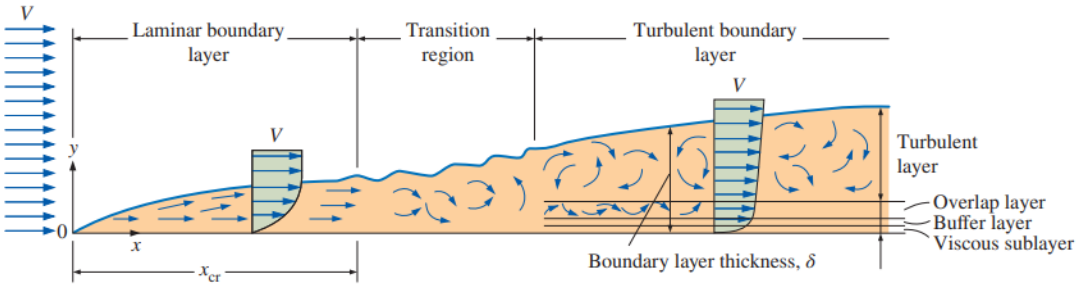

Figure 2: Flow developing from laminar to turbulent, figure taken from [24]

The $k-\epsilon$ turbulence model consists of two PDE's (partial differential equations), one which solves the turbulent kinetic energy (k) of the flow, and another which solves the rate of dissipation of the kinetic energy (ϵ) of the flow. The $k-\epsilon$ model is well established and is the most validated turbulence model used in CFD simulations. Compared to other turbulence models the $k-\epsilon$ model only needs initial and boundary conditions in order to run.

The standard $k-\epsilon$ turbulence model solves the two following equations:

$$\vartheta = k^{1/2} \tag{17}$$

$$\ell = \frac{k^{3/2}}{\epsilon} \tag{18}$$

where ϑ is the velocity scale, and ℓ is the length scale.

2.2 CFD modelling method

CFD software are powerful tools capable of solving turbulent flow numerically. Star-CCM+ is a finite volume method (FVM) based CFD software. This method divides the domain in question into discrete control volumes in such a way that the boundary for each control volume lies mid-way between adjacent nodes. In this way, each node is surrounded by either a control volume or cell.

2.2.1 Star-CCM+

3D models used in Star-CCM+ can either be drawn directly in the software using the 3D-CAD tool, or it can be drawn in other CAD software and then imported. For this thesis all models were drawn directly in Star-CCM+. A more detailed explanation of the following steps can be found in Hermansen [22].

The first step is to draw the boundary of the model. This is done by drawing a square in the XY-plane and then setting the lengths of the sides to the desired measurements. Once this is done the sketch can be extruded with the desired length in the Z-direction. This box represents the entire space one wishes to analyze and will contain all other shapes needed. The next step is to draw sketches of the outer and inner walls of the room. The difference in measurements between these two walls represents the thickness of the walls. Both the outer and inner sketch

needs to be extruded to the desired height. When extruding it is important to select 'none' under body interaction, as the bodies needs to be separate from each other in the beginning. The difference in height here represents the thickness of the ceiling. Finally the doorway between the outer and inner zone needs to be drawn. Sketch the doorway in the desired wall, making sure the thickness of the doorway is the same as the thickness of the wall. Then extrude the doorway to the wanted height. There are now four bodies to work with.

To create the walls and ceiling separating the outer and the inner zone the outer body needs to be subtracted from the boundary body. This is a boolean operation and can be done in the CAD editor in Star-CCM+. To create the doorway, the same procedure is repeated. The boundary body and the inner body can now be combined into one unit. Finally, the door is added to the model. In order to prevent collisions between solids during the simulation, there should be a small gap between the walls and the door. In this work, this gap was set to 1.0cm. When the door is extruded, make it 2.0cm lower than the doorway. Finally, the door body needs to be translated 1.0cm in the z-direction. There should now be a 1.0cm gap between the wall and door, as well as a 1.0cm gap between the floor and the top of the doorway, and the door. See figure 3 of what a model looks like when all these steps are done. See figure 4 for an overview of the different types of doors.

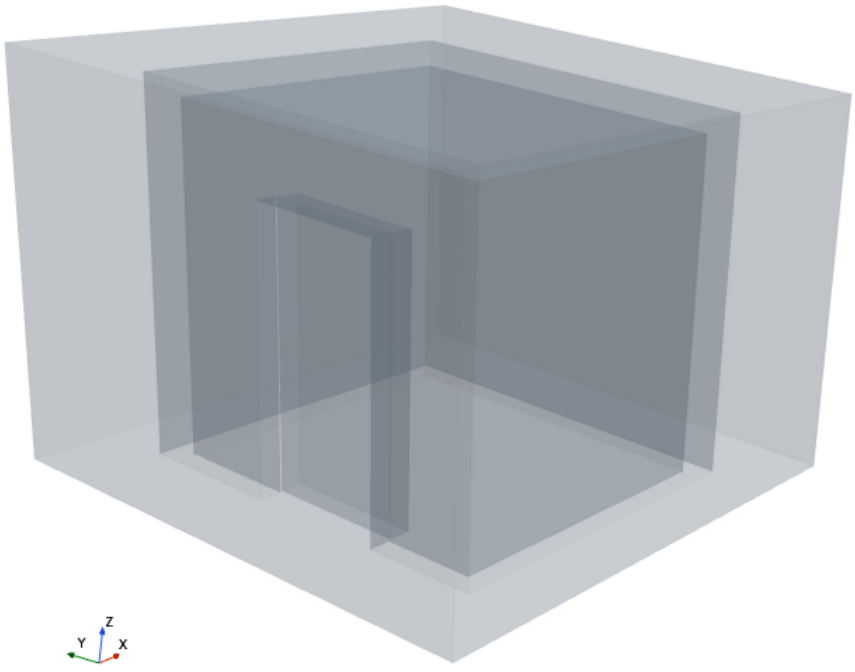

Figure 3: 3D CAD model drawn in Star-CCM+

These bodies can now be made into new geometry parts. Once the parts have been created, the surfaces can be split into patches. In addition to these parts, blocks needs to be added to the figure. These will be used to define areas around moving parts, and act as volumetic control areas where desired.

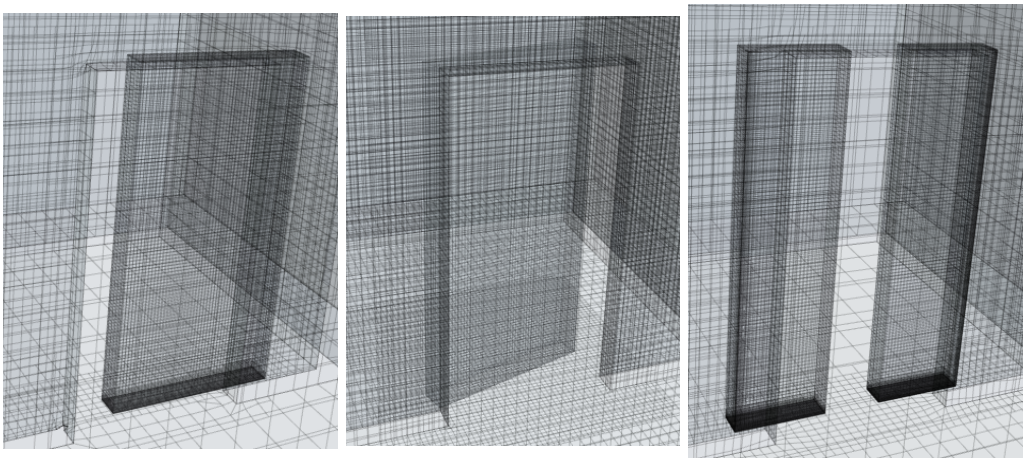

(a) Single sliding door (b) Hinged door (c) Double sliding doors

Figure 4: Mesh view of all three door types

All bodies that will be included in the simulation can now be assigned to regions. For regions with moving parts, the boundaries and motion specification needs to be edited. The boundary of the moving part should be kept as a wall-type, but the boundaries of the block needs to be changed to overset mesh. Under physical values motion specification needs to be changed to translation or rotation. This is explained further in section 2.2.3.

Now automated meshes can be created for all parts that will be included in the simulation. This is done under the parts menu. The following mesh models were used for this thesis:

- Trimmed cell mesher
- Surface remesher
- Prism layer mesher

Trimmed cell mesher defines the mesh by using cubes, and requires less computational power than other cell mesher options. Since time is a limitation, this model was selected. Prism layer mesher allows the user to define the size and the number of prisms in border regions. Surface remesher double-checks that surfaces in the models are valid, and improves quality if able. See figure 5 for examples of trimmed cell mesher and prism layers. It should be noted that a highly complex and detailed model does not automatically mean it is better, the focus of a good CFD model should be the quality of the mesh, not the size of it [24, chapter 15].

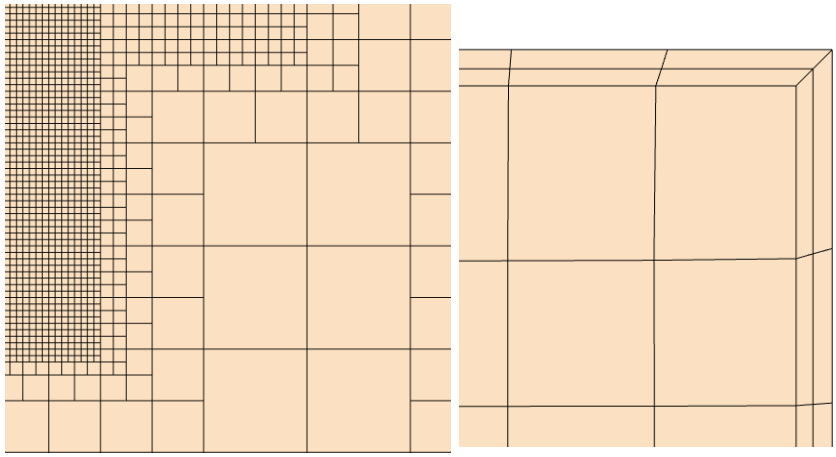

(a) Trimmed cells (b) Prism layer near border

Figure 5: Mesh view

In areas where extra attention to the mesh is desired, a volumetric control area can be defined. This is a subcategory of the automated mesh menu. A part, like a box or cylinder, needs to be created in the model where the volumetric control will be performed. This area should use the same mesh models as the other parts. In addition to these automated meshes, the overset mesh also needs to be created. The overset mesh has options to enable 'close proximity', 'alternate hole cutting', and 'prism layer shrinkage'. These should be enabled when there are parts near each other in the models.

Now the physics continua can be set up. See figure 6 for models used in this thesis. For this simulation the inner room will contain air and the corridor will contain tracer gas SF6, so multi-component gas needs to be selected. Air and SF6 are chosen from the gas component menu. The gases are defined under initial conditions using field functions. This is explained further in the field functions section.

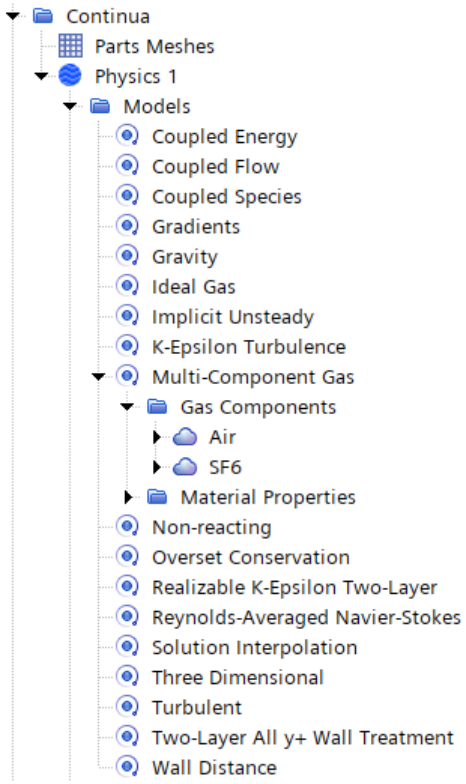

Figure 6: Physics models used in Star-CCM+

2.2.2 Derived parts

Plane sections were used to visualize the simulation. Three plane sections were created, one perpendicular to each of the axes. These were created under derived parts and were then applied to scalar and vector scenes. These scenes could then be set to show certain values throughout the simulations. These include velocity magnitude, temperature, and mass fraction for scalar scenes. For the vector scenes, velocity presented using Line Integral Convolution fields was selected.

2.2.3 Motion and field functions

There will be two types of body motion used in this thesis: translation and rotation. Translation will be used to simulate sliding type doors, and rotation will be used to simulate hinged type doors. Both of these motions can be defined in Star-CCM+. To define the opening and closing phases, field functions were used.

In Star-CCM+, field functions are a tool that can help define parameters in a simulation. There were two types of setups required for this simulation: defining the initial conditions of gases, and motion of solids. The initial concentration of air can be set by defining a volume in the model, in this case the inner zone. This zone is set to contain only air, while everything outside of the zone contains a set fraction of air. Hermansen [22] calculated the value for this fraction in their thesis, and it is assumed this value is valid for this work as well. The initial concentration of SF6 can be set by simply subtracting the field function for air from 1, see figure

7. When simulating a thermal case a similar field function can be defined for temperature, where the inner zone will have one temperature and the outer zone one will have another one. There will be no need to subtract this field function from another one, as both temperatures will be defined in this one.

The field functions used for movement of solids in this thesis all share the same core structure. In the case of doors, the solid needs to transform a set distance for its opening phase, then perform the same translation in reverse for its closing phase.

The following field function was used for the sliding door:

$$f(y) = \begin{cases} -0.5m/s, & 0 < t \leq 2s \\ 0.5m/s, & 2s < t \leq 4s \end{cases} \tag{19}$$

The field function defined by equation 19 was also applied to the double sliding door, with some modifications. The doors need to move opposite each other, so the top door starts by moving in the positive y-direction, then switching direction for its closing phase. The opposite setup is used for the other door. Their movement speed is also cut in half, to account for their smaller size.

The following field function was used for the hinged door:

$$f(\omega) = \begin{cases} -0.78rad/s, & 0 < t \leq 2s \\ 0.78rad/s, & 2s < t \leq 4s \end{cases} \tag{20}$$

YAir - Definition

```
($${Position}[0]> 1.8 && $${Position}[0]< 4.35 &&
$${Position}[1]> 0.65 && $${Position}[1]< 4.35 &&
$${Position}[2]< 2.6) ? 1:0.999412
```

YSF6 - Definition

```
1-${YAir}
```

Figure 7: Field functions for concentration of air and SF6

2.2.4 Wall functions

When calculating the main qualities - velocity, temperature, turbulent kinetic energy and dissipation rate - in the turbulent boundary inner layer wall functions provide algebraic approximations. These approximations are independent of the Reynolds numbers of the flow. At high Reynolds number one can assume that the rate of turbulence production equals the rate of turbulent dissipation.

Star-CCM+ has two wall functions available: standard and blended. The standard wall functions are specifically defined for the viscous sub-layer or the log layer, but does not cover the buffer layer. The blended wall function are continous and cover all three sub-layers. Functions used by Star-CCM+ are defined in the software's user guide [21].

2.2.5 Presentation grid

Presentation grids were added to the doorway for each simulation. A presentation grid is made up of small points, as seen in figure 8. The resolution of these points can be modified to the users need. A presentation grid can be defined to record many types of data across its area, such as velocity, temperature, mass fraction, and density. For this thesis the following resolution was used: $\Delta x = \Delta y = 0.02m$, giving 50 nodes in the X-direction and 100 nodes in the Y-direction.

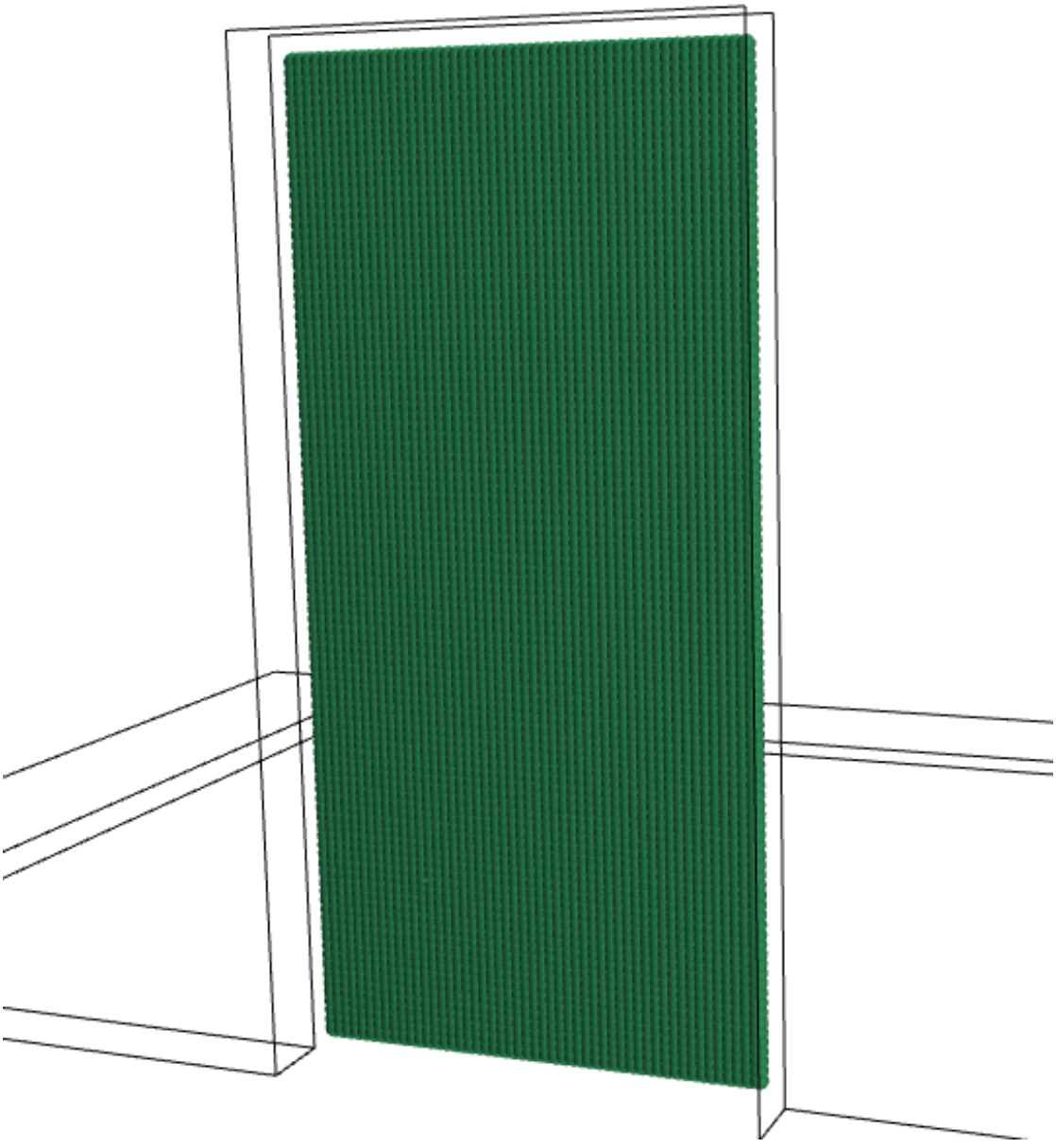

Figure 8: Presentation grid

Star-CCM+ was told to store this data in .csv (Comma Separated Values) tables which can then be imported into data analysing software for post-processing (see appendix D). The following formula is used when analysing the data from the tables:

$$\Phi(t) = \left[\oiint_A (\rho \varphi \vec{V} . \vec{n} dA) \right] dt \tag{21}$$

where ρ is density, $\vec{V}.\vec{n}$ is the normal velocity, and φ is an interchangeable variable, depending on what is being calculated. For this thesis this can be:

- $\varphi = 1$ for total mass
- $\varphi =$ Mass fraction of SF6 for mass of SF6
- $\varphi = C_p T$ for energy

2.3 MATLAB

MATLAB is a numeric computing software developed by Mathworks. This software allows for large tables to be plotted into graphs, which makes it very useful for these types of problems [25].

To analyse the data from the presentation grid a post-processing two types of scripts were written in MATLAB (see appendix C). 2D line plots were used to plot step-wise and cumulative values. Delaunay triangulation was used to reconstruct contours from the transient data at the doorway. These plots were defined so that they look out from the inner zone.

2.4 Use of supercomputer

Due to the complexity of CFD models, calculation time is often an issue. For spring of 2022, the Department of Civil Engineering and Energy Technology at OsloMet was granted access to the super-computer cluster Fram hosted at UiT Arctic University of Norway [26]. This powerful hardware drastically reduced the time required to run simulations.

Submissions to this supercomputer was done via a SSH client. The simulation file was uploaded to their servers, and then submitted as a job. The name of the job had to be specified, along with the number of nodes and CPU hours (CPUh) required (see appendix A).

3 Verification model

In this section the verification model is explained. Additionally, preliminary results obtained from both the simulations and post-processing of the verification model are discussed. It is important to have such a model in order to verify the CFD method being used. The verification model is similar in shape to the case model used in this thesis. The size of the verification model is smaller than the case model, this was done to reduce the computational time needed.

3.1 Verification in Star-CCM+

The verification model consists of an inner and an outer room separated by a door. The size of the inner zone does not allow for the sliding door to fully open. Given that this is a verification model, it is assumed to not be an issue. The measurements of the model are listen in table 1.

Table 1: Dimensions of the verification model

	Width [m]	**Length [m]**	**Height [m]**
Boundary	3.60	3.80	3.00
Outer wall	2.26	2.70	2.6
Inner wall	2.11	2.55	2.45
Door	0.15	1.00	1.98
Double sliding doors	0.15	0.5	1.98

The three validations models have different cell counts. This is in part because the volumetric control areas are different: it is bigger in the hinged door model, as it needs to cover a larger area inside the inner zone. Another reason is that the mesh for the hinged door is finer than the mesh of the other two. Initially when making the models their regions had identical mesh setups. However, this resulted in mesh gaps for the hinged door. The mesh grid can be seen in figure 9. Mesh cell counts for all three models are listed in table 2.

Table 2: Cell count for the verification models

Model	**Cell count**
Sliding door	400,539
Hinged door	673,221
Double sliding doors	529,740

The coordinates for the three views are:

- xz plane at y = 1.90m (figure 9a)
- yz plane at x = 0.81m (figure 9b)
- xy plane at z = 1.00m (figure 9c)

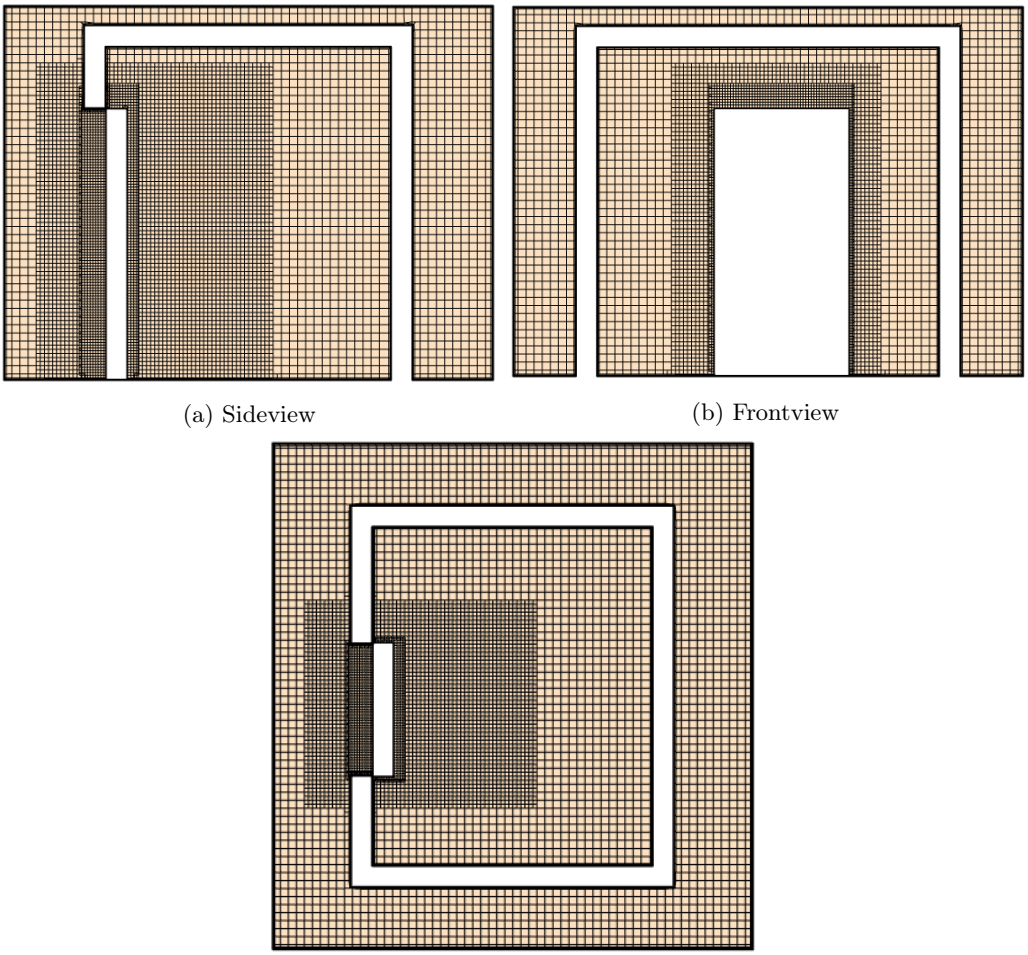

(a) Sideview (b) Frontview

(c) Topview

Figure 9: Mesh grid for verification model, hinged door

The mesh setup used in the verification models are listed in table 3.

Table 3: Mesh setup, verification model

Area	Base size [cm]	No. of prism layers [-]	Max cell size [%]
Background	20	3	100
Volumetric control	8	5	-
Doorway	2	5	100

These cell counts are within range of what previous studies have used [7, 11].

The initial conditions for all three verification models are listed in table 4. There are no inlets or outlets considered in this model. Fluid flow will be generated by the motion of the door, and

will be turbulent and coupled. At the model initialization the inner room will only contain air while all SF6 gas will be located in the outer room, see figure 10. Since no thermal analysis is done in the verification models the standard temperature of 300K is used, a pre-set by Star-CCM+ when making a new model. All solid surfaces are considered to be adiabatic. Scalar and vector scenes are seen from z = 1.0m. All initial conditions used in the verification models are listed in table 4.

Table 4: Initial conditions for verification models

Condition	**Value**
Pressure	101325Pa
Species specification	Mass fraction
Temperature	300K
Turbulent specification	$K + \epsilon$
Turbulent dissipation rate	$1.0e^{-6}$ m^2/s^3
Turbulent kinetic energy	0.001 J/kg
Velocity	[0.0, 0.0, 0.0] m/s

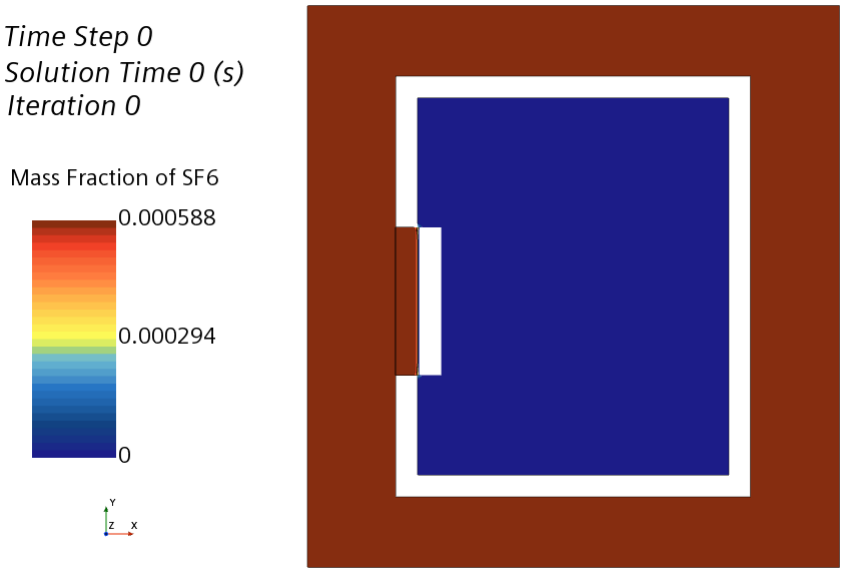

Figure 10: Validation model when initialized

All three models are set to simulate four seconds, the door opening during the first 2 seconds and closing during the last 2 seconds. The timestep for both simulations was set to 0.005 seconds, and each timestep has 10 iterations.

3.2 Results for sliding type door

Figure 11 shows the scalar and vector field during the door's opening phase. In figure 11a we can see a small amount of tracer gas starting to enter the inner zone. From figure 11b vorticity generated by the movement of the door is evident.

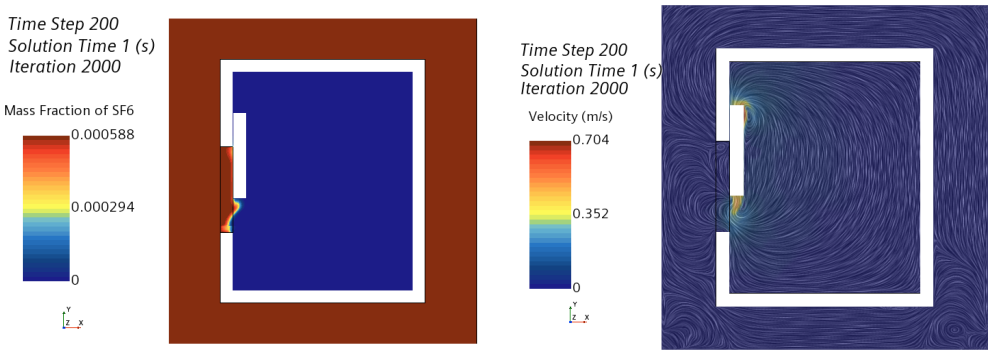

(a) Scalar field (b) Vector field

Figure 11: Sliding door when opening at t = 1.0s

The sliding door in its fully opened state is show in figure 12. As can be seen in figure 12a, there is still little tracer gas entering the inner zone. The tracer gas that does enter the inner zone does so near the middle of the doorway. Looking at figure 12b vorticity can be seen in both the inner and the outer zone. The highest velocity can be found in the northbound area of the door. Here the door and the wall is in close proximity, which could explain the velocity we see here.

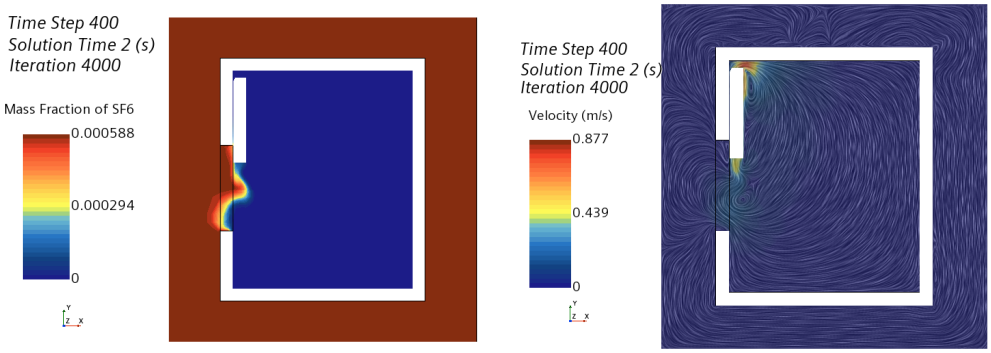

(a) Scalar field (b) Vector field

Figure 12: Sliding door when fully open at t = 2.0s

Figure 13 depicts the scalar and vector fields for when the door is closing. From figure 13a it is obvious that SF_6 has entered the inner zone, flowing along the door surface facing into the zone. Comparing this area to figure 13b, there is a clearly defined vortex at this location. There is also an area with relatively high velocity following in the path of the moving door. From observation there seems to be little air leaving the inner zone.

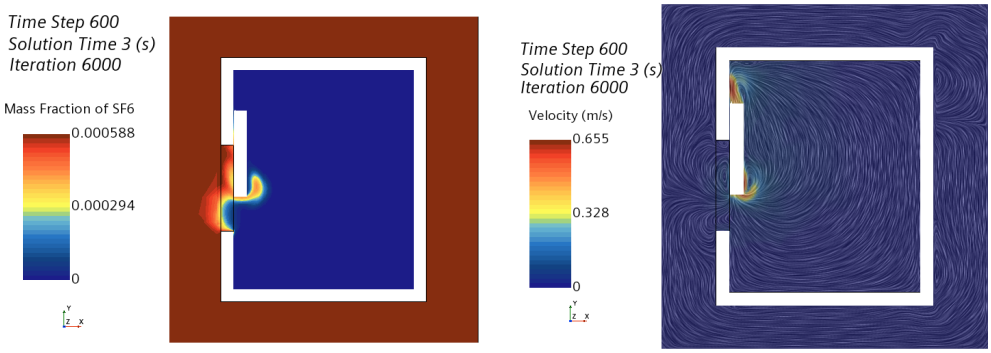

(a) Scalar field (b) Vector field

Figure 13: Sliding door when closing at t = 3.0s

In figure 14 we see the scalar and vector fields for the sliding door when fully closed. Figure 14a shows that what SF_6 that has entered the inner zone is located around the door. Small amounts of air can now be seen on the other side of the door. From figure 14b it is clear that the vortexes around the door remain.

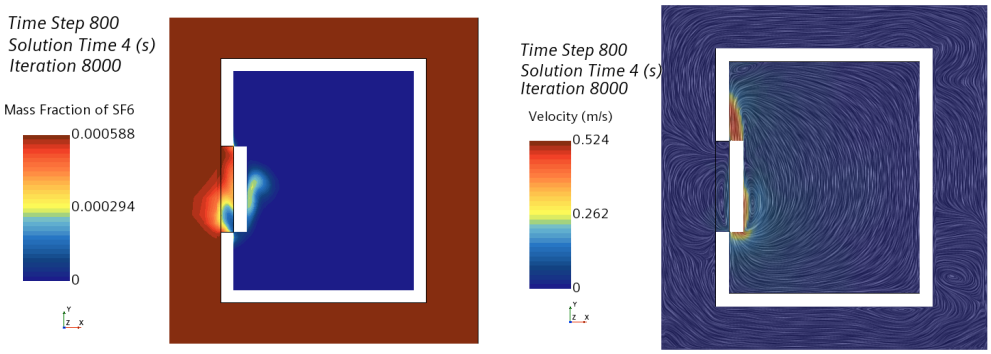

(a) Scalar field (b) Vector field

Figure 14: Sliding door when fully closed at t = 4.0s

From figure 15a we can see a global maximum at t $\approx$ 2.1s and a global minimum at t $\approx$ 2.0s, with $1.09e^{-7}$ kg and $-4.63e^{-7}$ kg of SF_6 transferred respectively. The global minimum occurs right after the door has started closing. It is assumed that this minimum point is due to the door pushing it back out. Comparing the mass of SF_6 exchanged to the average velocity we see that the graphs are similar. This makes sense as air velocity is the only influence on fluid movement in these simulations. The velocity at the global minimum is -0.043 m/s, while at the global maximum it is 0.012 m/s.

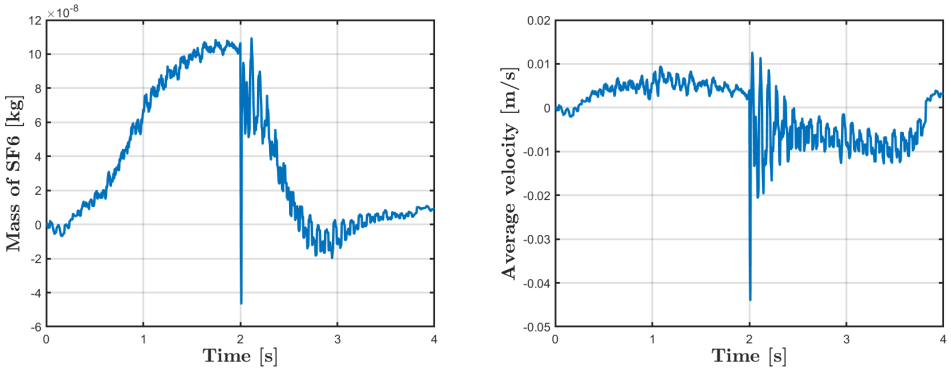

(a) Mass of SF6 exchanged (b) Average velocity

Figure 15: Sliding door graphs

Figure 16 shows the graph for cumulative mass of SF_6 exchanged. This graph tells us that a total of $2.87e^{-5}$ kg of SF_6 passed through the doorway. Overall the transfer of SF_6 through the doorway has been positive. A slight decrease can be seen at t $\approx$ 2.6s. This coincides well with the negative mass exchange value explained in figure 15a.

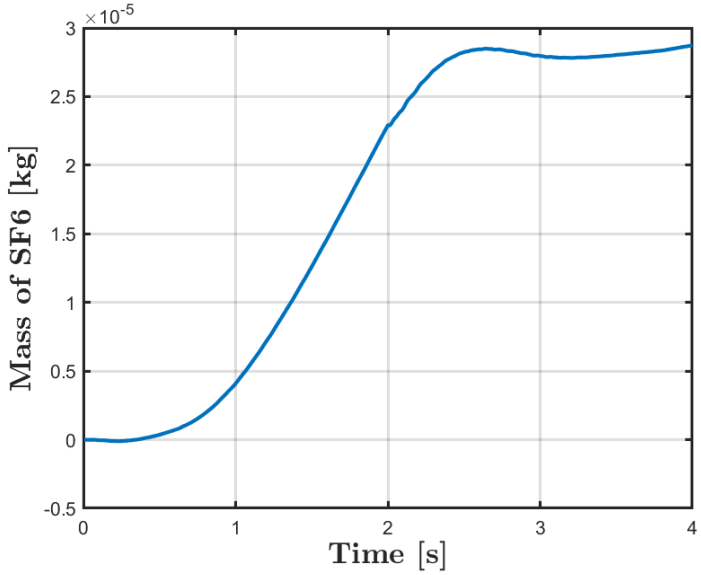

Figure 16: Cumulative amount of SF_6 for sliding door

3.3 Results for hinged type door

Figure 17 illustrates the scalar and vector fields for the hinged door as it is opening. Compared to the sliding door we can see a drastic increase in both amount of tracer gas entering the inner zone and vorticity. The vortexes around the door match up well with where we can see tracer gas entering.

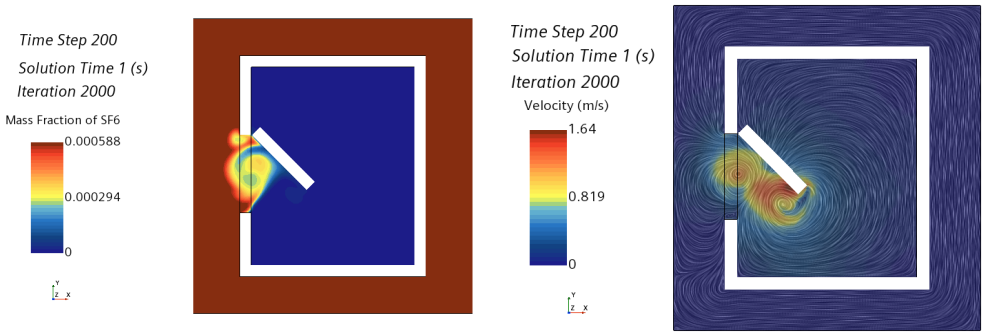

(a) Scalar field

(b) Vector field

Figure 17: Hinged door when opening at t = 1.0s

In figure 18 we see the scalar and vector fields for the hinged door when it is fully opened. From figure 18a we can see tracer gas having been dragged well into the room by the movement of the door. Comparing this vector field to that of the sliding door this is a much more chaotic picture. Noticeable vortexes have been generated all throughout the inner zone, as well as around the doorway in the outer zone.

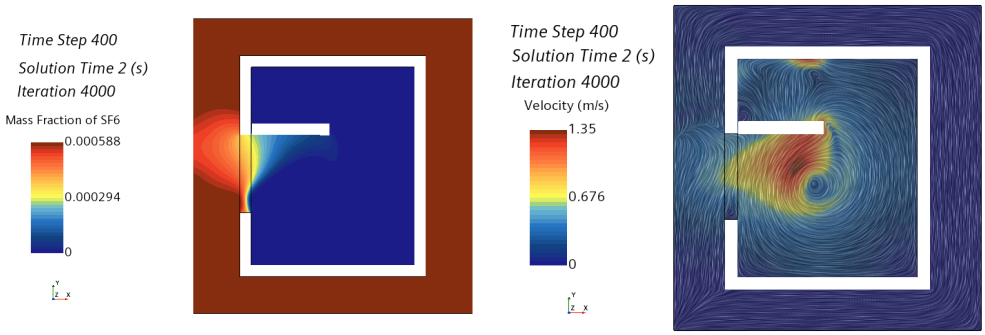

(a) Scalar field

(b) Vector field

Figure 18: Hinged door when fully opened at t = 2.0s

Figure 19 depicts the scalar and vector fields for the hinged door as it is closing. Figure 19a shows a clear "tongue" of SF_6 gas sticking into the inner zone. There are also traces of SF_6 gas inside the inner zone. The vector field shows much more activity than its sliding door counterpart. From observation there seems to be a greater number of vortexes, with clearly higher velocities. There is also a greater amount of air entering the outer zone.

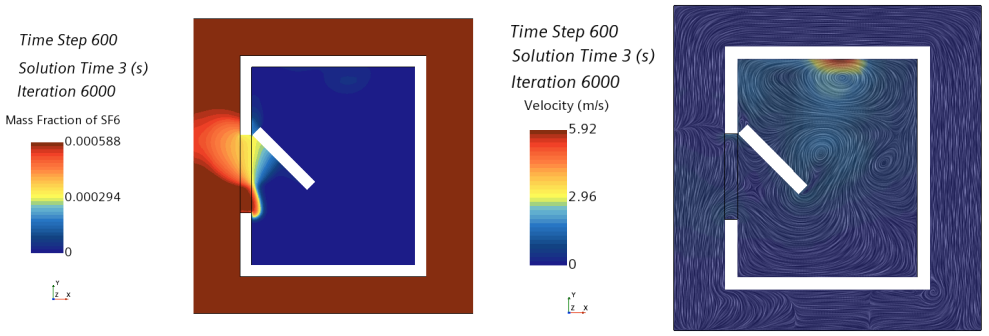

(a) Scalar field

(b) Vector field

Figure 19: Hinged door when closing at t = 3.0s

In figure 20 the scalar and vector fields for when the hinged door is fully closed can be seen. Figure 20a shows traces of SF_6 gas being spread out in the inner zone, most noticeably by the southern wall. Figure 20b now shows two vortexes inside the inner zone. The southernmost of these two is clearly the largest, and it coincides well with the location with the highest amount of SF_6 gas.

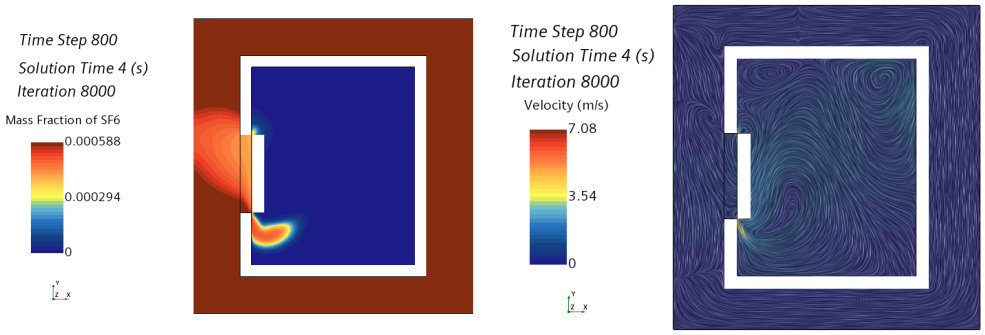

(a) Scalar field

(b) Vector field

Figure 20: Hinged door when fully closed at t = 4.0s

Figure 21 shows the graphs plotting the mass exchange of SF6 and the average fluid velocity throughout the simulation. From figure 21a it is clear that already at the very start of the simulation we achieve the global maximum, with $1.39e^{-6}$ kg of SF_6 being exchanged. At this time the average velocity was 0.38 m/s. Fascinatingly, the global minimum does not occur until the very end of the simulation, with $-9.15e^{-7}$ kg of SF_6 being exchanged. At this time the average velocity was -0.32 m/s. There are also a local minimum and local maximum that should be noted. At t $\approx$ 2.7s we have a local minimum with $-6.43e^{-7}$ kg of SF_6 being exchanged, with an average velocity of -0.34 m/s. At t $\approx$ 2.8s we have a local maximum with $8.0e^{-7}$ kg, and an average velocity of 0.48 m/s.

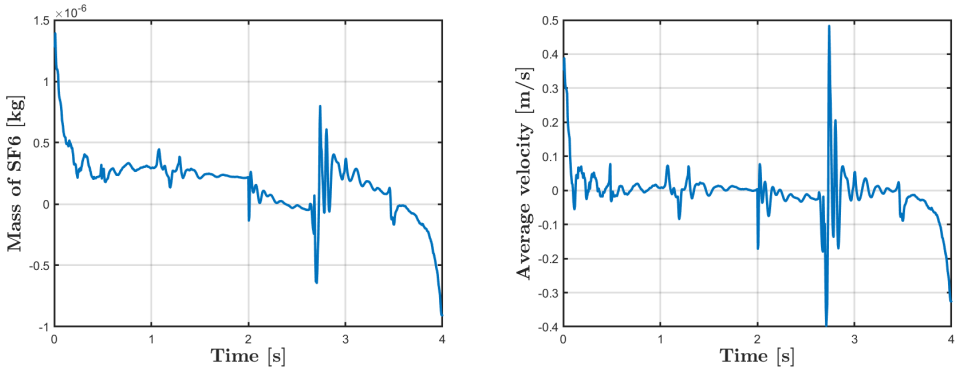

(a) Mass of SF6 exchanged (b) Average velocity

Figure 21: Graphs for hinged door

In figure 22 we see the graph showing the total mass of SF_6 exchanged through the doorway. Reading the graph we see that a total of $1.3e^{-4}$ kg entered the inner zone. It is interesting to see that between t $\approx$ 0.1s and t $\approx$ 2.0s the amount of SF_6 entering the inner zone is almost linear. Around t $\approx$ 2.8s there is a small decrease in the amount of SF_6 mass. It is possible that this is due to the door pushing the gas out, before vortexes generate enough air velocity to start dragging the gas back in again. From t $\approx$ 3.5s and up to the end of the simulation we see a decrease of SF_6 mass. It is obvious that this decrease is due to the motion of the closing door, pushing SF_6 back out to the outer zone.

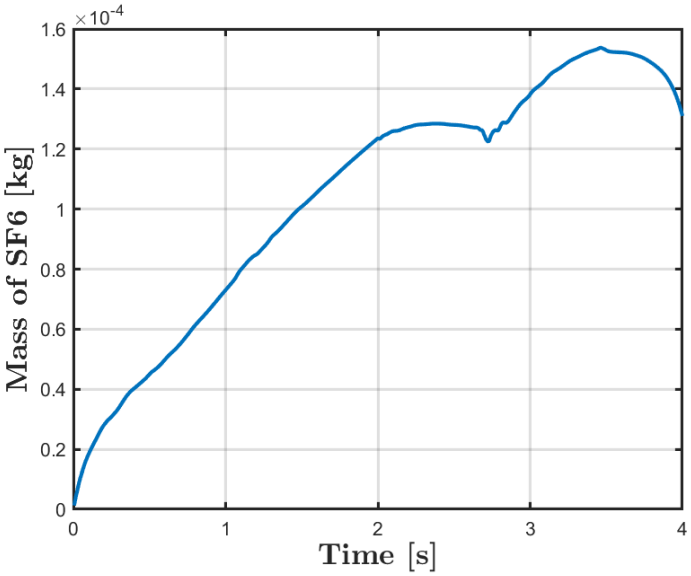

Figure 22: Cumulative amount of SF_6 for hinged door

3.4 Results for double sliding doors

Several of the fields around the doors from this simulation have small areas where the mesh is not always defined. These show up at random timesteps in the simulation as small and/or thin white areas. Since the dimensions of the zones are identical and the size of the mesh around the door is similar to the two previous simulations these are assumed to be graphical glitches, and will not affect the results obtained.

In figure 23 we see the scalar and vector fields for when the double sliding doors are opening. From figure 23a it is clear that no SF_6 gas has made it past the actual doorway threshold yet. Examining figure 23b we do see very noticeable vortexes being generated in the middle of the doorway. Comparing this to the previous two simulations it is evident that the hinged door still has the most turbulent flow.

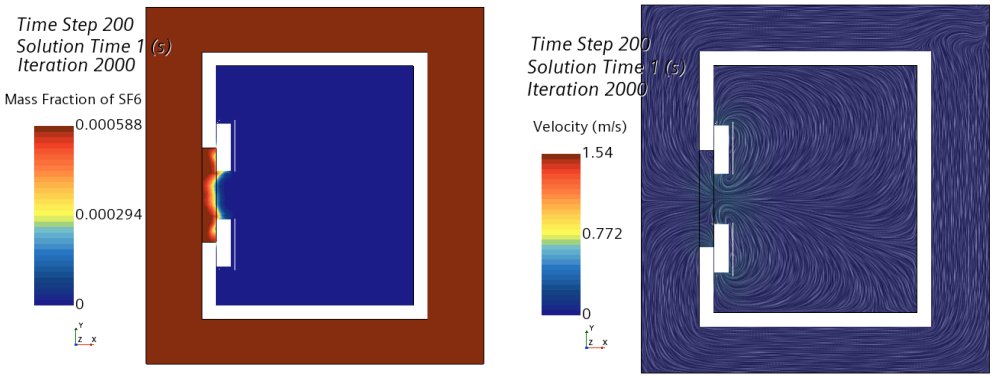

(a) Scalar field

(b) Vector field

Figure 23: Double sliding doors when opening at t = 1.0s

Figure 24 depicts the scalar and vector fields for when the double sliding doors are fully opened. Examining figure 24a we can now see SF_6 gas has started entering the inner zone. In figure 24b we see that the fluid velocity is approximately the same as in the previous figure. The vector field around the doorway coincides well with where we see SF_6 enter the inner zone. It is assumed that there is now sufficient vortex generation in the doorway for SF_6 gas to be dragged into the inner zone.

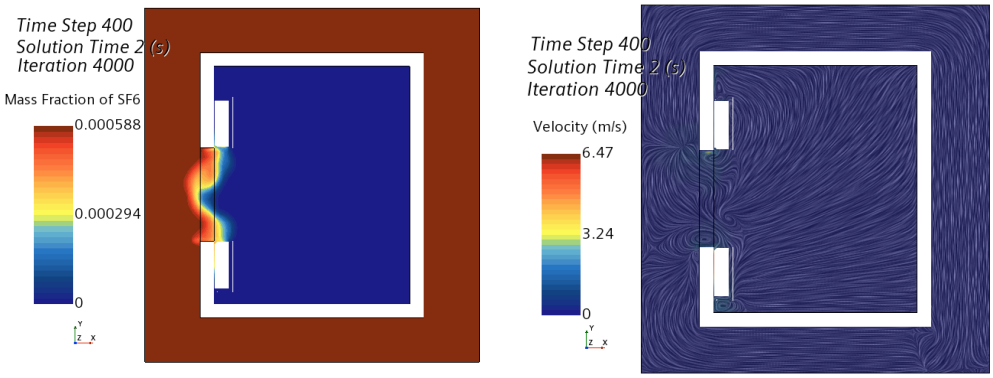

(a) Scalar field (b) Vector field

Figure 24: Double sliding doors when fully opened at t = 2.0s

Figure 25 shows the scalar and vector field for when the double sliding doors are closing. Looking at figure 25a we now see that SF_6 gas have entered the inner zone, in a similar manner as we saw in the simulation for the single sliding door. From figure 25b we can now see many clearly defined vortexes both in the inner and the outer zone. Especially around the doorway these vortexes are assumed to give good conditions for mixing of fluids. This matches with what we can see in the scalar field.

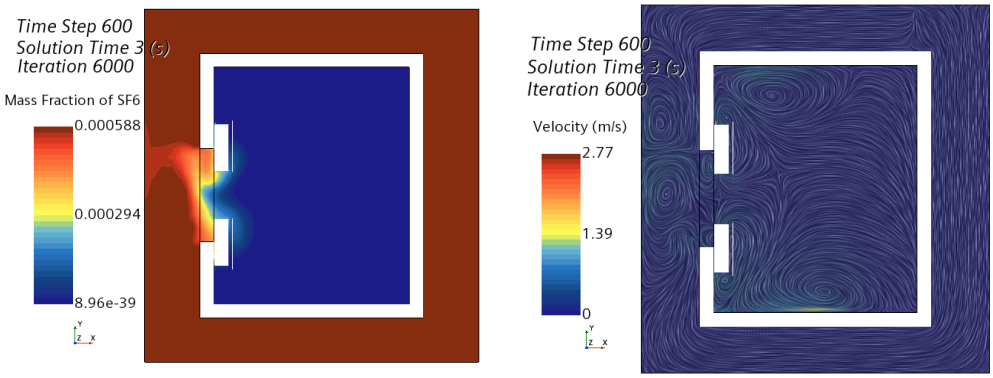

(a) Scalar field (b) Vector field

Figure 25: Double sliding doors when closing at t = 3.0s

In figure 26 we see the scalar and vector field for when the double sliding doors are fully closed at the end of the simulation. Examining the scalar field we see that SF_6 gas is present in the inner zone. We also see that there are trace amounts of air that have entered the outer zone. Comparing this to the vector field we see that the air velocity is highest in the small gap between the two doors. This could be the cause for both mass flux into and out of the inner zone. We also see that the most defined vortexes are located in the inner zone. It is possible that these could lead to further mixing of fluids in this zone as more time progresses.

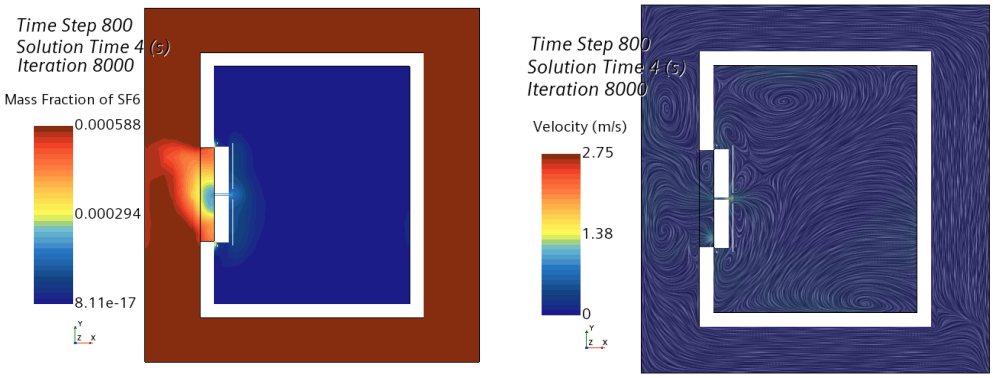

(a) Scalar field (b) Vector field

Figure 26: Double sliding doors when fully closed at t = 4.0s

Figure 27 shows the graphs plotting the mass of SF_6 exchanged and the average velocity through the doorway throughout the simulation. From figure 27a we can see that at most, $1.19e^{-6}$kg of SF_6 was exchanged. This occured at t $\approx$ 2.0s, a short moment after the doors had started closing. At this time the average air velocity was 0.51m/s, which is also the global maximum. We can also see that just before the doors were fully open, $8.51e^{-7}$kg of SF_6 was exchanged. At this time the average air velocity was 0.27m/s.

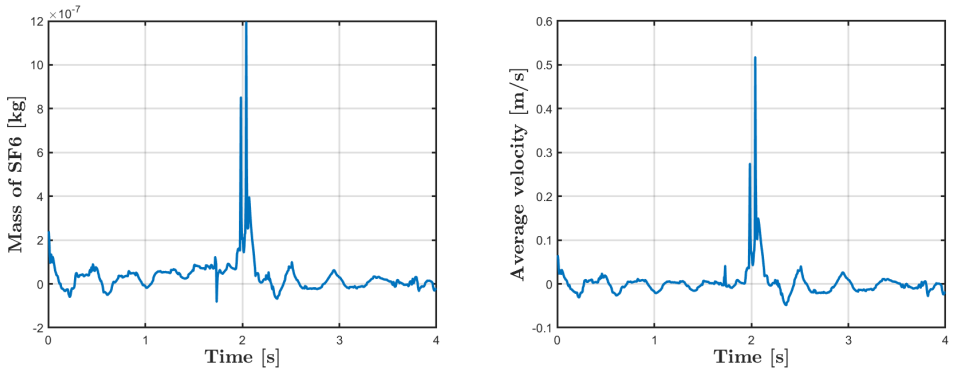

(a) Mass of SF6 exchanged (b) Average velocity

Figure 27: Graphs for double sliding doors

In figure 28 we can see the cumulative mass of SF_6 exchanged through the doorway. Reading the graph we see that a total of $2.79e^{-5}$kg of SF_6 was exchanged. It shows that the most amount of mass was exchanged between t $\approx$ 1.1s and t $\approx$ 2.0s. It is interesting to note that very little mass is entering the inner zone during the doors closing phase.

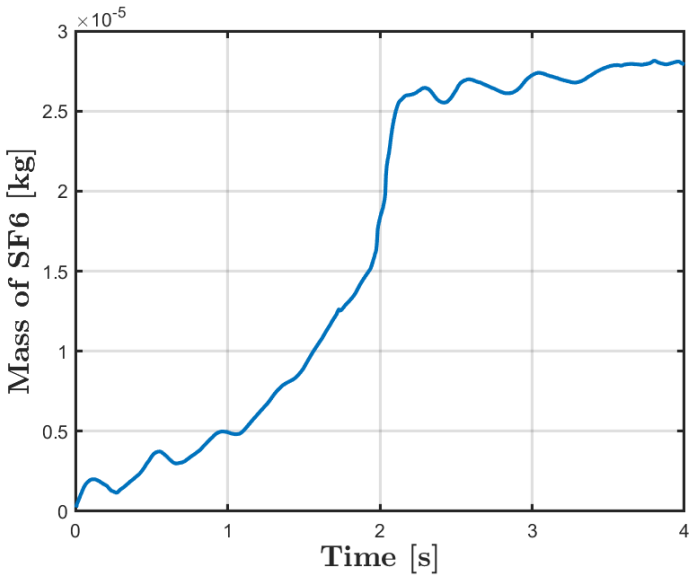

Figure 28: Cumulative amount of SF_6 for double doors

3.5 Summary of results from verification models

The results for mass transfer from all three simulations are listed in 5. From this it is clear that the hinged type door had the most mass transferred through the doorway. It can also be seen that the double sliding doors transferred the least amount of mass.

Table 5: Comparison of validation simulations

Door type	Total mass SF6 exchanged [kg]
Sliding	$2.87e^{-5}$
Hinged	$1.30e^{-4}$
Double sliding	$2.79e^{-5}$

For run time of each simulation, see appendix E. For residuals, see appendix B.2

3.6 Previous studies

The results found for sliding and hinged doors in these validation models match with previous studies [16, 19, 22]. The hinged type door shows greater fluid velocity both in the outer and inner zone, as well as an increased mass exchange through the doorway. The case models in this thesis will advance the previous study done by Hermansen [22] by increasing the mesh, as well as introducing human motion.

4 Case model

In this section the case models and their setup are explained. These models will consider three different types of doors: single sliding, hinged, and double sliding. For each case a simplified model of a person moving through the doorway as it opens and closes will also be included.

4.1 Problem setup

Like the verification model, this model consists of two zones separated by a wall with a doorway being the only entry-point between the them. The dimensions used in the case models are listed in table 6.

Table 6: Dimensions of the case model

	Width [m]	**Length [m]**	**Height [m]**
Boundary	5.00	5.00	3.00
Outer wall	2.85	4.00	2.85
Inner wall	2.55	3.70	2.60
Door	0.15	1.00	1.98
Double sliding doors	0.15	0.5	1.98

In addition to door motion human movement was introduced. A simplified model of a human being will be placed in front of the doorway, and will move from the outer to the inner zone as the door is opening. There will also be thermal analysis included in these three simulations.

The model person used for these simulations was drawn in Star-CCM+ using cylinders. Table 7 lists the measurements used.

Table 7: Dimensions of the model person

	Height [m]	**Radius [m]**
Legs	0.65	0.08
Torso	0.60	0.23
Arms	0.50	0.06
Head	0.20	0.09

These measurements are in no way taken to be accurate, but are only used to model the rough shape and form of a human being.

The mesh will be similar for all three simulations. The mesh is most refined around the door, doorway, and the person, as these are the areas of the greatest interest for this thesis. In addition, three custom volumetric control areas have been defined: one covering the movement of the door, one covering the movement of the person, and one for refining the mesh around the door. All of these will vary in size and form, depending on what type of door is being simulated. In the case of the sliding door, the control volume will follow along the side of the wall that the door is moving parallel to. Similarly, in the case of the double sliding doors the control volume will follow along either side of the doorway, as this door will move along both sides simultaneously.

In the case of the hinged door, the control volume will cover an area going into the inner zone. The control volume covering the person will be identical for both the sliding and the double sliding doors: it will cover a straight path into the inner zone. For the hinged door the control volume needs to be altered to account for how the person moves in this simulation. The person will move into the inner zone during the opening phase of the door, then move directly away from the door for one second, then continuing to move into the zone. This was done to avoid collisions between the door and the person. Figure 29 shows the volumetric control areas used in the hinged door simulations, as seen in a mesh view.

These three views were used for all scalar and vector scenes in the simulations and were placed at the following coordinates:

- xz plane at y = 2.50m (figure 29a)
- yz plane at x = 1.85m (figure 29b)
- xy plane at z = 1.00m (figure 29c)

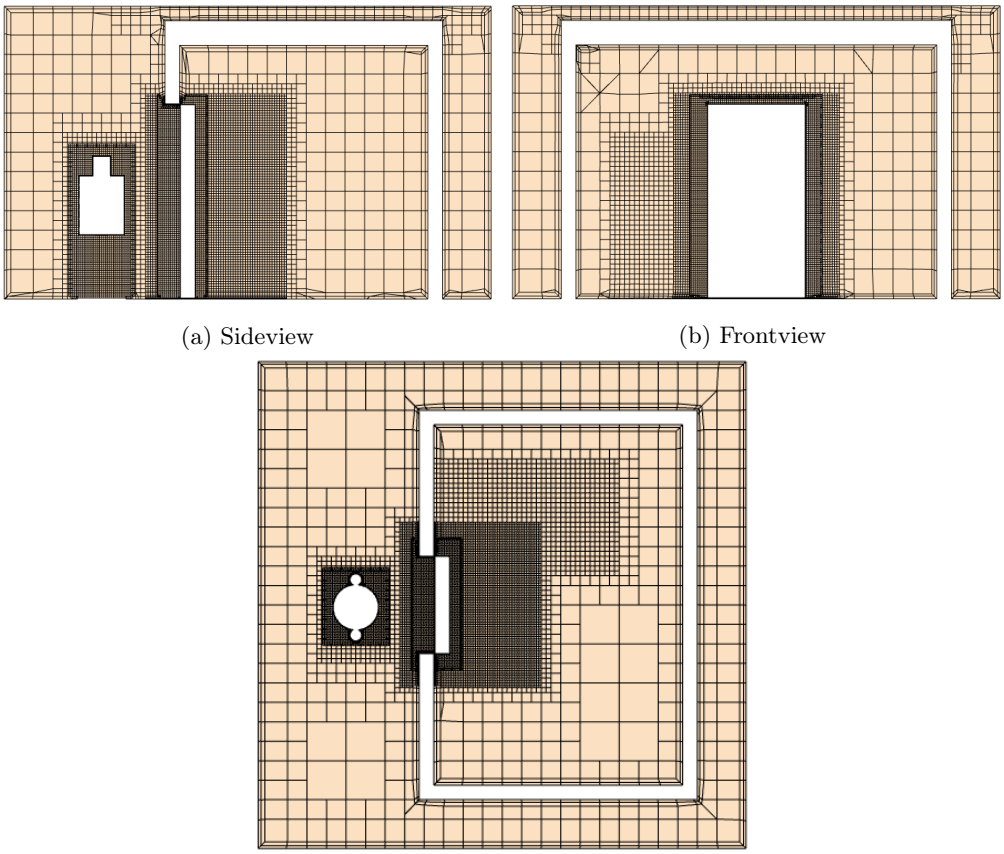

(a) Sideview (b) Frontview

(c) Topview

Figure 29: Mesh grid for hinged door model

Table 8: Mesh setup, case model

Area	Base size [cm]	No. of prism layers [-]	Max cell size [%]
Background	20	3	10000
Volumetric control	4	5	-
Doorway	2	2	100

The mesh setup used for the case models are listed in table 8

As stated above, the case models included a thermal analysis for each door type used. The temperature of the person moving through the doorway will be set to that of an average human being, 310K. This temperature can be set from the regions initial conditions category. These simulations do not last long enough to get any noticeable heat-plumes rising from the model person, but it was included to add more realism to the simulations. The outer zone will have an initial temperature of 293K while the inner zone will have an initial temperature of 253K, as seen in figure 30.. Both of these temperatures are defined using field functions. The initial conditions used in the case models are listed in table 9.

Table 9: Initial conditions for case models

Condition	Value
Pressure	101325Pa
Species specification	Mass fraction
Temperature	Field function
Turbulent specification	$K + \epsilon$
Turbulent dissipation rate	$1.0e^{-6}m^2/^3s$
Turbulent kinetic energy	0.001 J/kg
Velocity	[0.0, 0.0, 0.0] m/s

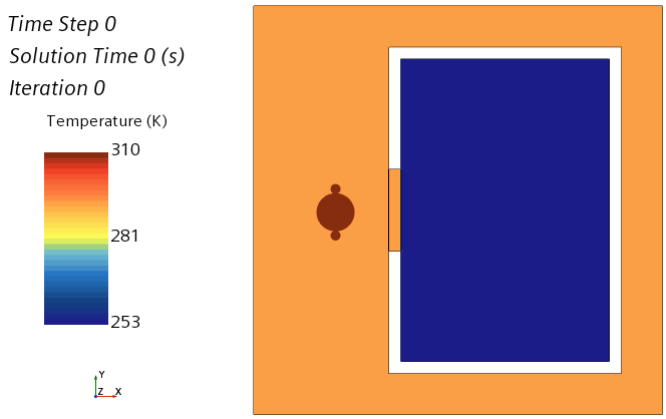

Figure 30: Scalar field showing temperature of initialized model

When drawing double sliding doors in Star-CCM+ two smaller blocks are drawn, placed at the same location as the one solid block used for the hinged and sliding door. These two parts can then be assigned to their own two regions, which allows them to move independently of each other.

The cell count for the different types of doors will differ, as they will require different volumetric control areas. The cell count for each of the models is listed in table 10.

Table 10: Cell count for the case models

Model	**Cell count**
Sliding door	1,134,543
Hinged door	1,001,956
Double sliding doors	1,340,047

These cells counts are within range of what previous studies have used [2, 10].

5 Results and discussion

In this section the results of the three different case models are discussed. Scenes including mass fraction, vector, and temperature taken from Star-CCM+ at different timesteps are presented and analysed. Data collected from Star-CCM+ have been post-processed in MATLAB into graphs and Delaunay triangulation figures, which are also presented and analysed here. Thermal analyses of all three cases are presented in their own sections.

5.1 Results for sliding door

Figure 31 shows the scalar and vector fields for the sliding door while it is opening. In figure 31a trace amounts of SF_6 can be seen starting to entering the inner zone. Comparing this to figure 31c it is clear that air has started entering the outer zone via the bottom of the doorway. Comparing the scalar fields to figure 31b we see that the vorticity around the door and doorway match with where the gas is entering. From the the vector field we can also clearly see the outline of the moving person.

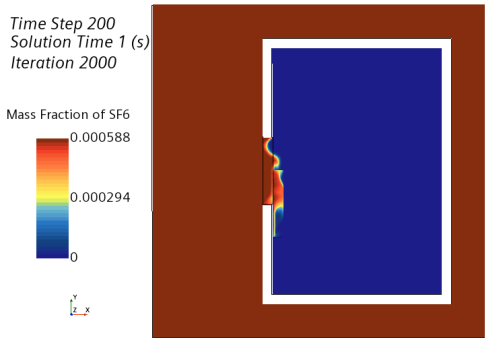

(a) Scalar field, top view

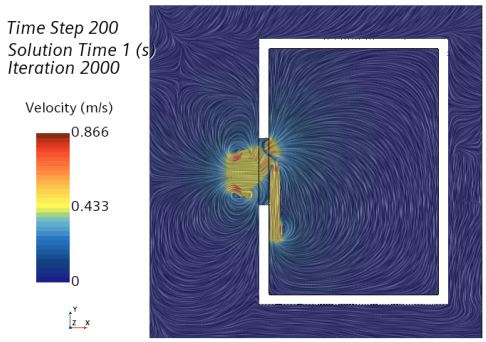

(b) Vector field, top view

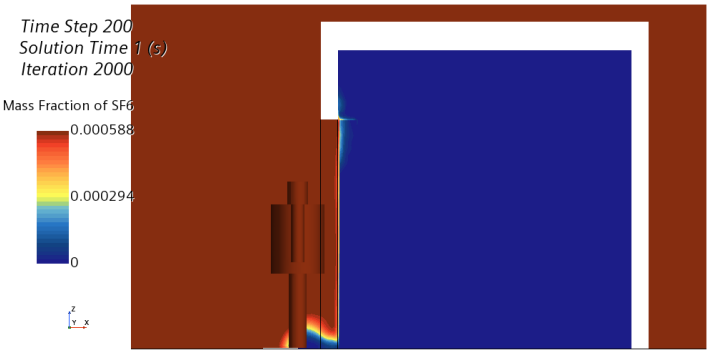

(c) Scalar field, side view

Figure 31: Sliding door when opening at t = 1.0s

In figure 32 we see the scalar and vector fields for the sliding door when it is fully opened. The outline of the moving person is now more prominent in the scalar field, and looks to be dragging SF_6 into the inner zone. Figure 32c shows that SF_6 has started to rise in the inner zone. This

figure also clearly depicts mixing layers between air and SF_6 in both the inner and the outer zone. Figure 32b illustrates vorticity is of relatively high velocity in the doorway.

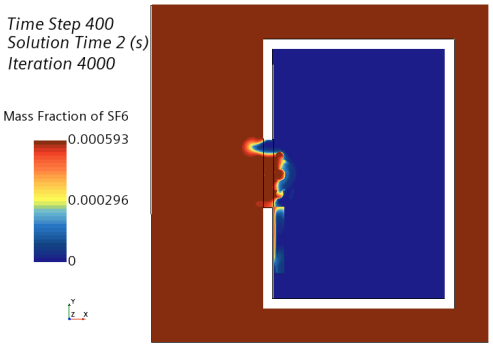

(a) Scalar field, top view

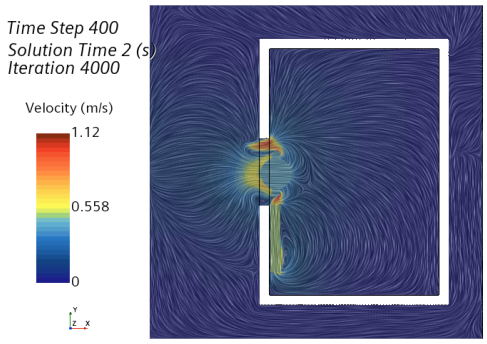

(b) Vector field, top view

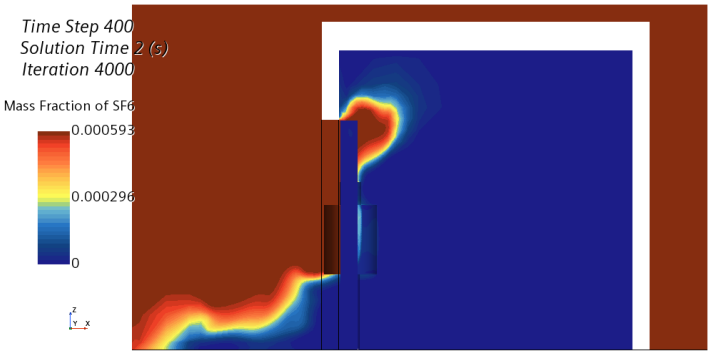

(c) Scalar field, side view

Figure 32: Sliding door when fully opened at t = 2.0s

Figure 33 shows the scalar and vector fields for the sliding door while it is closing. Examining figure 33a we can now clearly see SF_6 being dragged into the inner zone in the wake of the moving person. In figure 33c SF_6 can be seen along the back of the person, and starting to settle in the ceiling of the inner zone. Figure 33b shows very little vorticity, but with high air velocity between the moving door and the person.

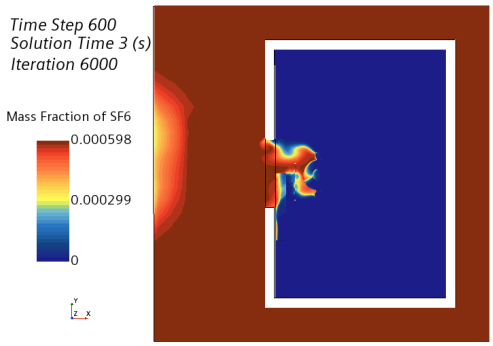

(a) Scalar field, top view

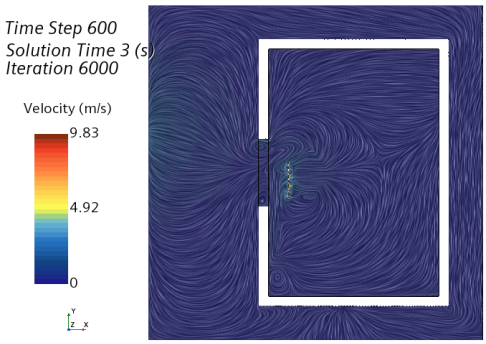

(b) Vector field, top view

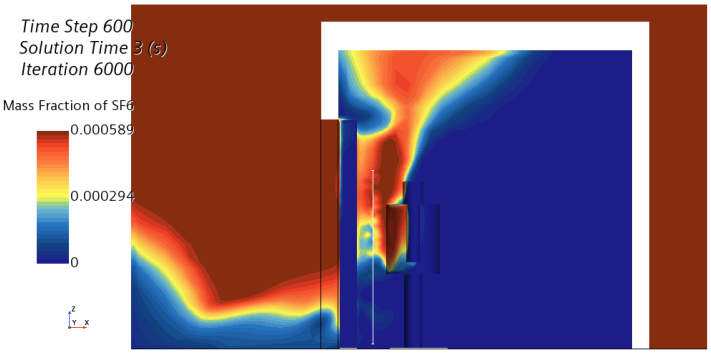

(c) Scalar field, side view

Figure 33: Sliding door when closing at t = 3.0s

In figure 34 we see the scalar and vector fields for the sliding door when it is fully closed. From figure 34a it is clear that there is trace amounts of SF_6 are the inner zone, concentrated around the door and the person. We can also see that a significant amount of air has entered the outer zone. In figure 34c we can see traces of SF_6 rising from the person. Figure 34b shows that there are high velocity vortexes around the door and person in the inner zone. We can also see vorticity in the upper left corner of the outer zone.

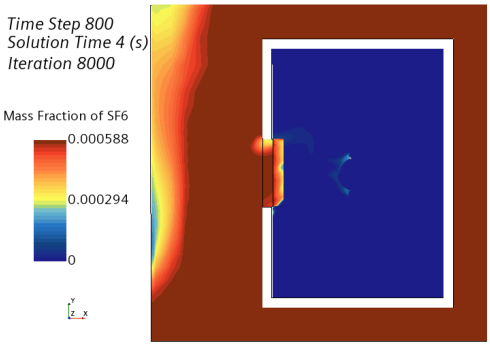

(a) Scalar field, top view

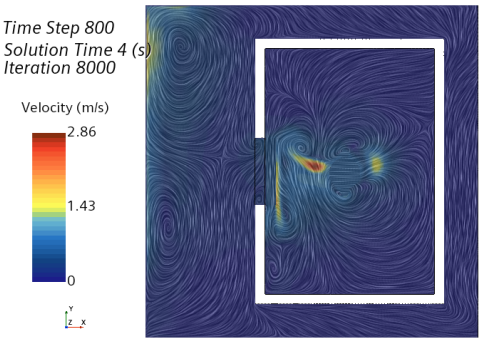

(b) Vector field, top view

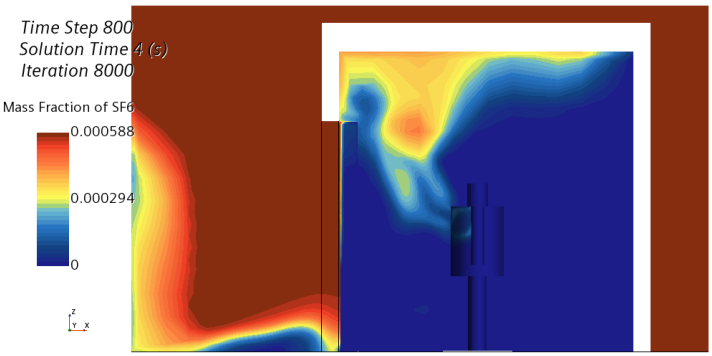

(c) Scalar field, side view

Figure 34: Sliding door when fully closed at t = 4.0s

Figure 35 show Delaunay plots, henceforth referred to as contour plots, for the mass fraction of SF_6 at given times through the doorway. Here we see that the SF_6 tends to enter in the top half of the doorway, and the air tends to leave in the bottom half, which agrees with the scalar side view figures. The movement of the door can be visualized by noting where air is allowed to pass into the outer zone.

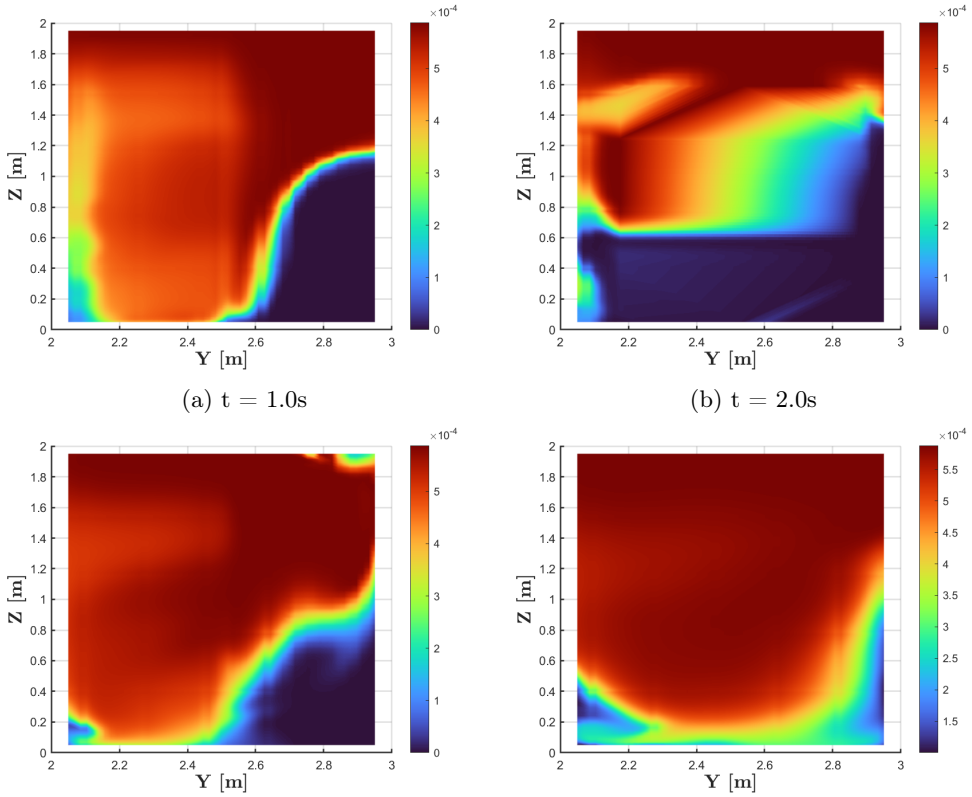

(a) t = 1.0s (b) t = 2.0s

(c) t = 3.0s (d) t = 4.0s

Figure 35: Mass fraction contours for sliding door

Contour plots showing air velocity can be seen in figure 36. In figure 36b we can see the negative velocity in the bottom half and the positive velocity in the top half. This match with how we see the fluids enter and leave the inner zone.

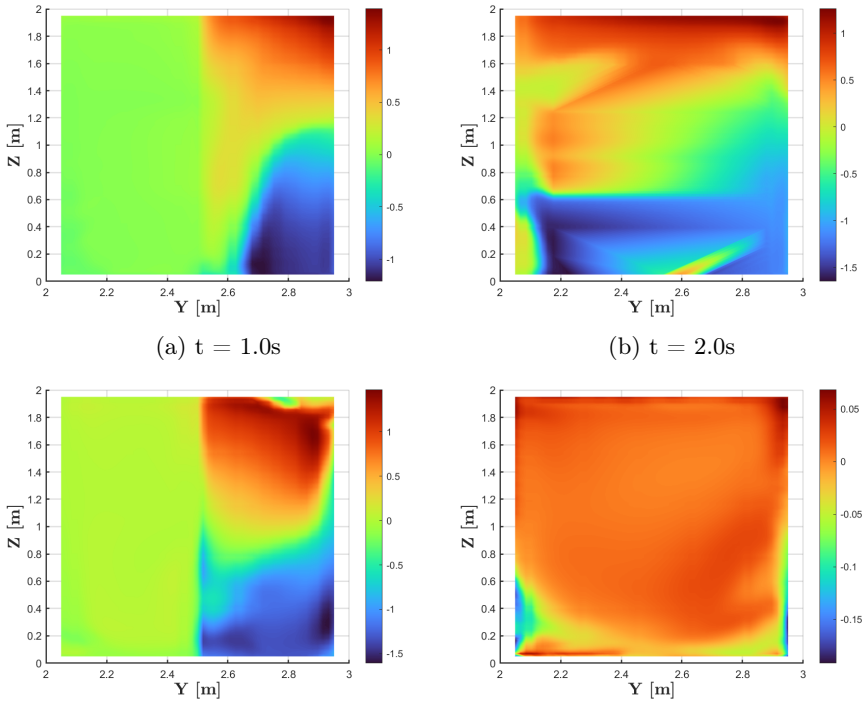

(a) t = 1.0s (b) t = 2.0s

(c) t = 3.0s (d) t = 4.0s

Figure 36: Velocity contours for sliding door

Figure 37 shows 2D line plots for mass of SF_6 exchanged and the average velocity through the doorway. From figure 37a we see that at most $6.20e^{-05}$kg was exchanged during the simulation. This exchange occured at t $\approx$ 2.7s. Compared to the rest of the graph, we see that during this time there is a relatively large spike in mass transferred. In figure 37b the average air velocity is presented. We can see that the global maximum velocity occurs at about the same time as the global maximum for mass transferred. At this point the velocity was 0.16m/s. There is a global minimum at t = 2.5s where the velocity was -0.075m/s, and a local minimum at t = 3.0s which achieves almost the same velocity. The cumulative mass of SF_6 transferred is shown in figure 37c. We see that there is a rather sharp increase in the amount of mass transferred at around t = 2.5s. Reading the graph we see that a total of 0.010kg of SF_6 was transferred through the doorway.

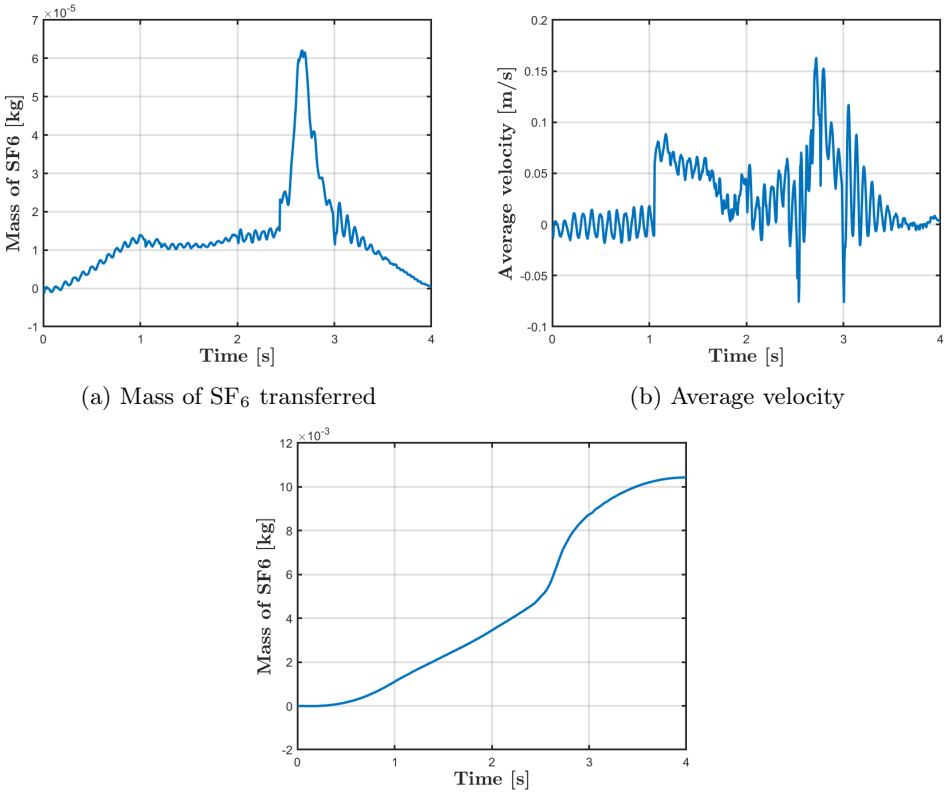

(a) Mass of SF_6 transferred

(b) Average velocity

(c) Cumulative SF_6 for sliding door

Figure 37: 2D line plots showing mass transfer and velocity for sliding door

5.1.1 Thermal results

In figure 38 we see four scalar fields showing temperature. Figure 38b cold air can be seen leave the inner zone, which matched what we saw in figure 32a. In figure 38c we see that a plume of heat is following in the wake of the moving person. At the end of the simulation we see small areas in the inner zone where the temperature has increased. We also see that there are parts of the outer zone where the temperature has decreased.

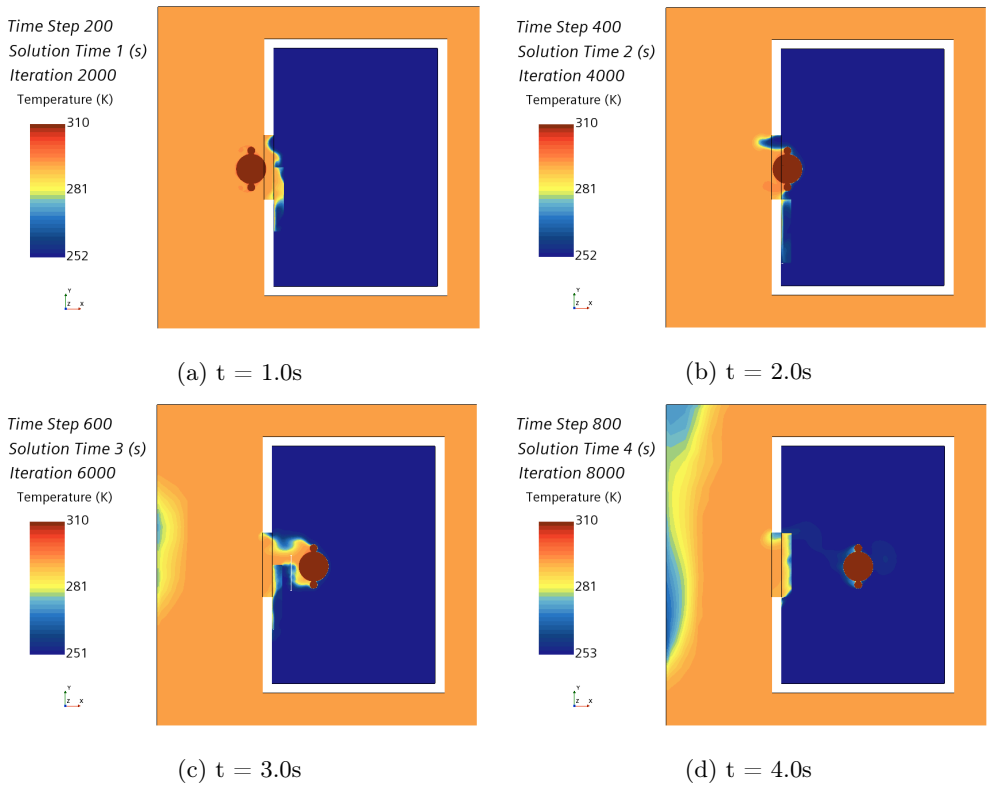

(a) t = 1.0s (b) t = 2.0s

(c) t = 3.0s (d) t = 4.0s

Figure 38: Scalar fields for sliding door with $\Delta T = 40°C$

Figure 39 show contour plots illustrating temperature contours through the doorway at given times. Here it is clear that the warm SF_6 of the outer zone enter through the top half of the doorway, and the cold air of the inner zone leave through the bottom half, with a mixing layer acting as a boundary layer between them.

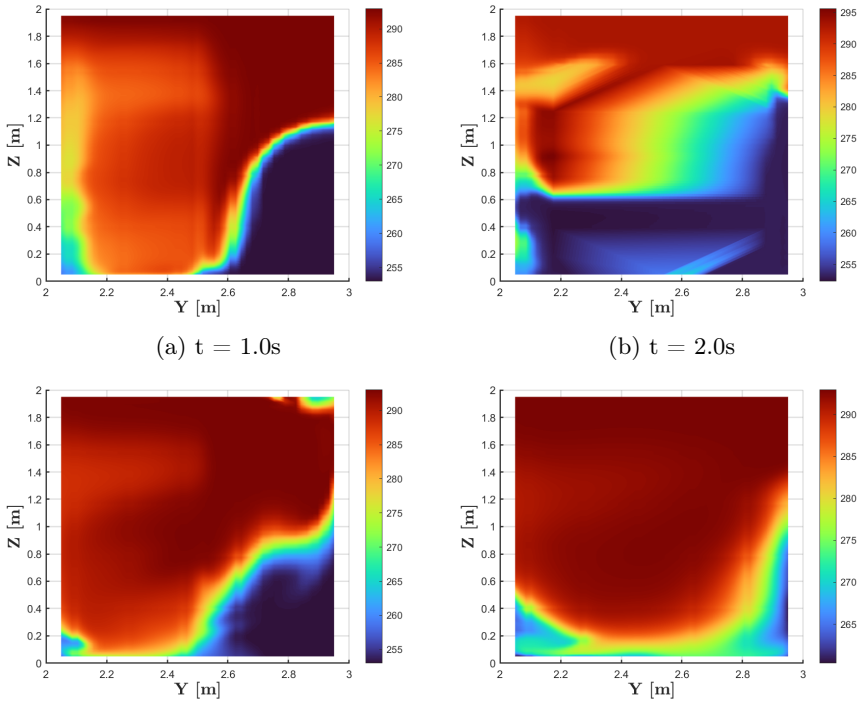

(a) t = 1.0s (b) t = 2.0s

(c) t = 3.0s (d) t = 4.0s

Figure 39: Temperature contours for sliding door

Figure 40 shows 2D line plots for energy transferred through the doorway. From figure 40a we see a global maximum at t = 2.8s with 7,44kJ of energy transferred. We have a global minimum at t = 3.0s with -3.45kJ energy transferred. There is also a local minimum at t = 2.5s with -3.44kJ energy transferred. Figure 40b tells us that a total of 0.917MJ of energy was transferred.

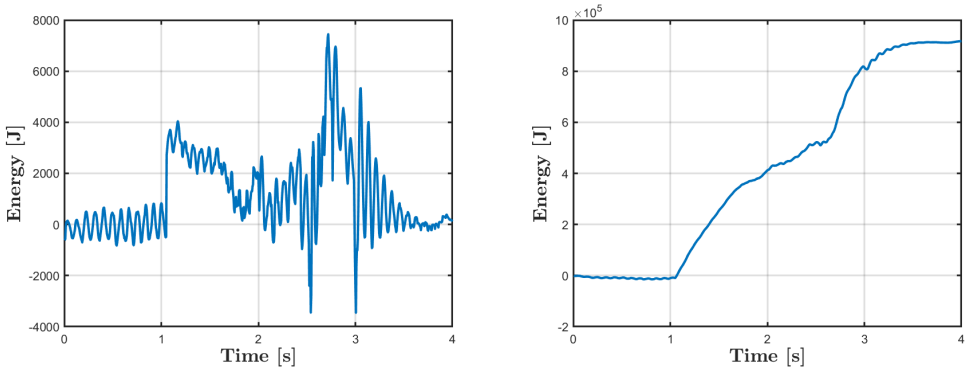

(a) Energy transferred (b) Cumulative energy transferred

Figure 40: 2D line plots for sliding door showing energy transfer

5.2 Results for hinged door

Figure 41 shows the scalar and vector fields for the hinged door while it is opening. From both figure 41a and 41c we can see that SF_6 has started entering the inner zone. Compared to the figures we saw for the sliding door, there is already significantly more activity in this simulation. From figure 41b we can also see that there is more vorticity than in the sliding door model, as well as higher air velocity.

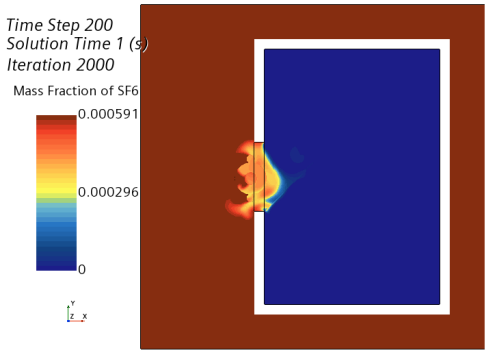

(a) Scalar field, top view

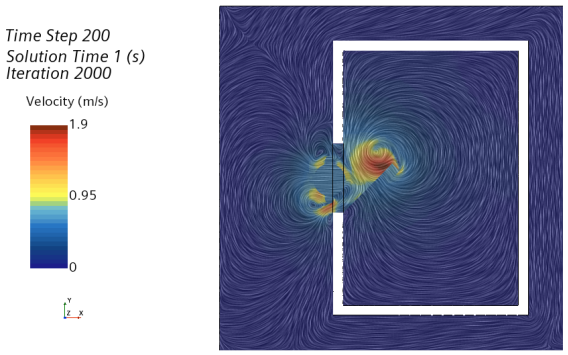

(b) Vector field, top view

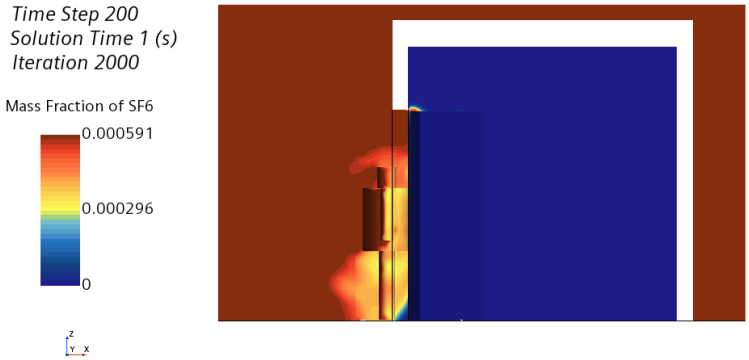

(c) Scalar field, side view

Figure 41: Hinged door when opening at t = 1.0s

Figure 42 depicts the scalar and vector fields for the hinged door while it is fully opened. From figure 42a the SF_6 can be seen entering the inner zone, following the movement of the person and the door, while on the opposite side of the doorway we see air entering the outer zone. In figure 42c it can be clearly seen that air is flowing out of the inner zone in the bottom of the doorway. In figure 42b vorticity caused by the moving door is evident, but that there is also significant vortex generation in the doorway which lines up well with where the air is leaving the inner zone.

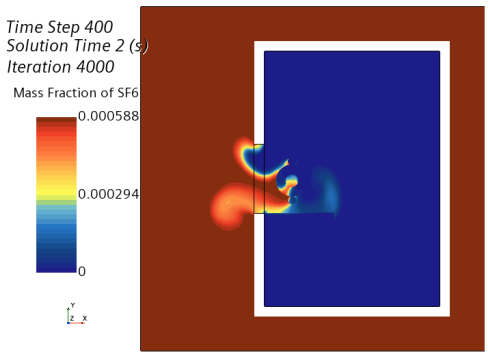

(a) Scalar field, top view

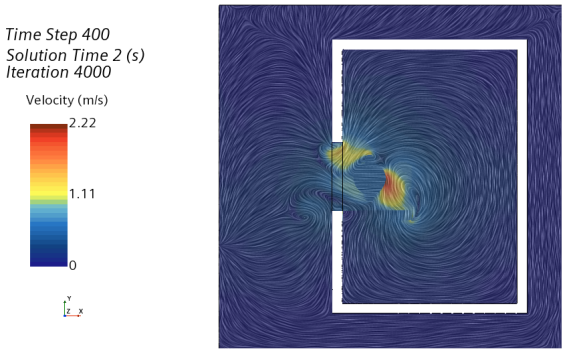

(b) Vector field, top view

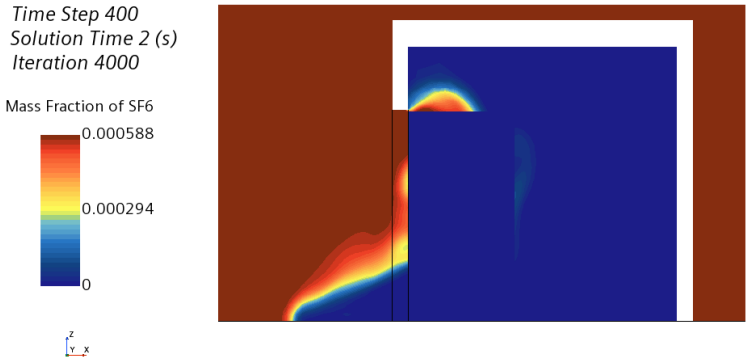

(c) Scalar field, side view

Figure 42: Hinged door when fully opened at t = 2.0s

Figure 43 shows the scalar and vector fields for the hinged door while it is closing. In figure 43a it is clear that a cloud of SF_6 has fully entered the inner zone behind the closing door. We can also observe a small amount of gas that is following the moving person. In figure 43c the SF_6 rising towards the ceiling can be seen. This figure also gives a clear view of mixing layers in the outer zone. From figure 43b it is evident that vorticity around the door remains. There is also noticeable vorticity around the moving person. Compared to the sliding door simulation there is significantly more activity happening here.

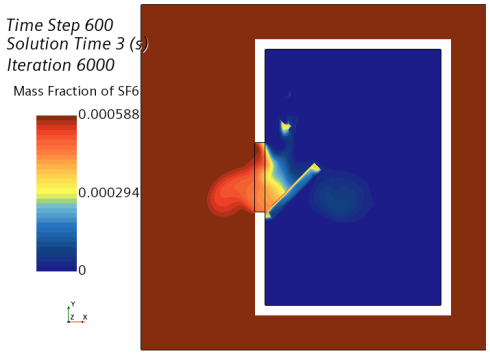

(a) Scalar field, top view

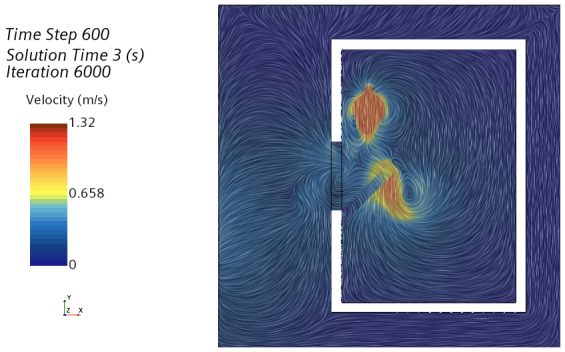

(b) Vector field, top view

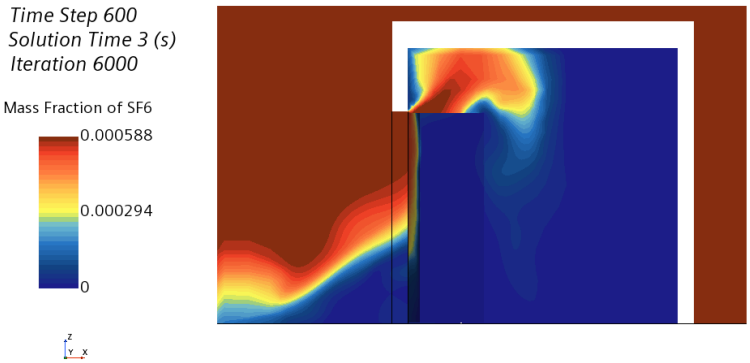

(c) Scalar field, side view

Figure 43: Hinged door when closing at t = 3.0s

In figure 44 the scalar and vector fields for the hinged door while it is fully closed can be seen. Figure 44a clearly shows a "tongue" of SF_6 sticking out from the door in the inner zone. A small cloud of SF_6 can also be observed following in the wake of the moving person. In figure 44c we can see that SF_6 has settled across the ceiling. Here we can also see the development of the mixing layers in the outer zone. Examining figure 44b it is evident that the only noteworthy vortexes are located around the closed door.

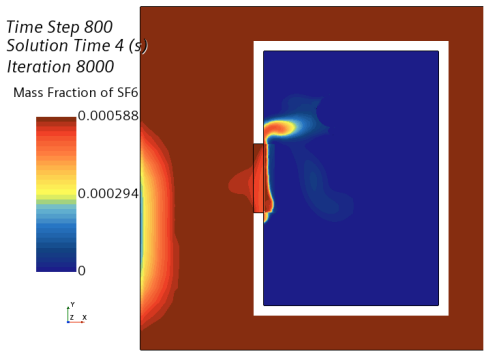

(a) Scalar field, top view

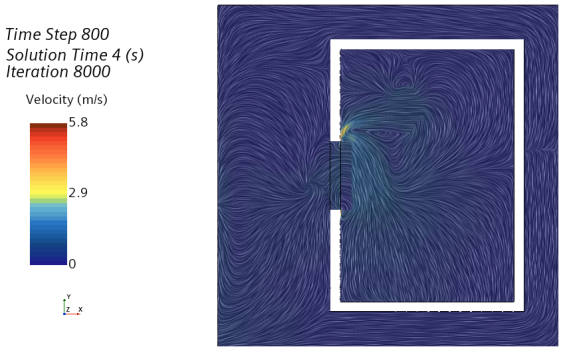

(b) Vector field, top view

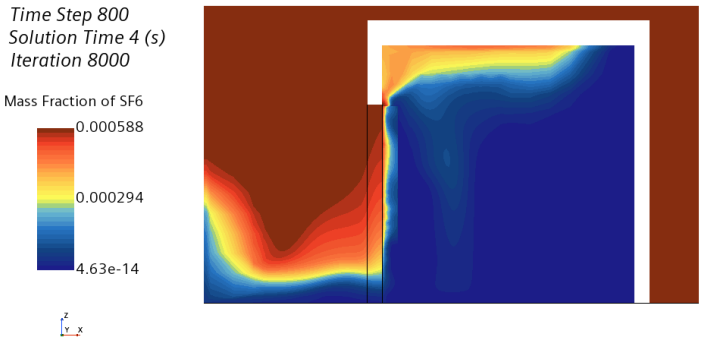

(c) Scalar field, side view

Figure 44: Hinged door when fully closed at t = 4.0s

Figure 45 show contour plots for the mass fraction of SF_6. Like the scalar side view figures showed, SF_6 tends towards entering in the top half and air tends towards leaving in the bottom half of the doorway. It is interesting to note that in figure 45a there are mixing layers throughout almost the entire doorway.

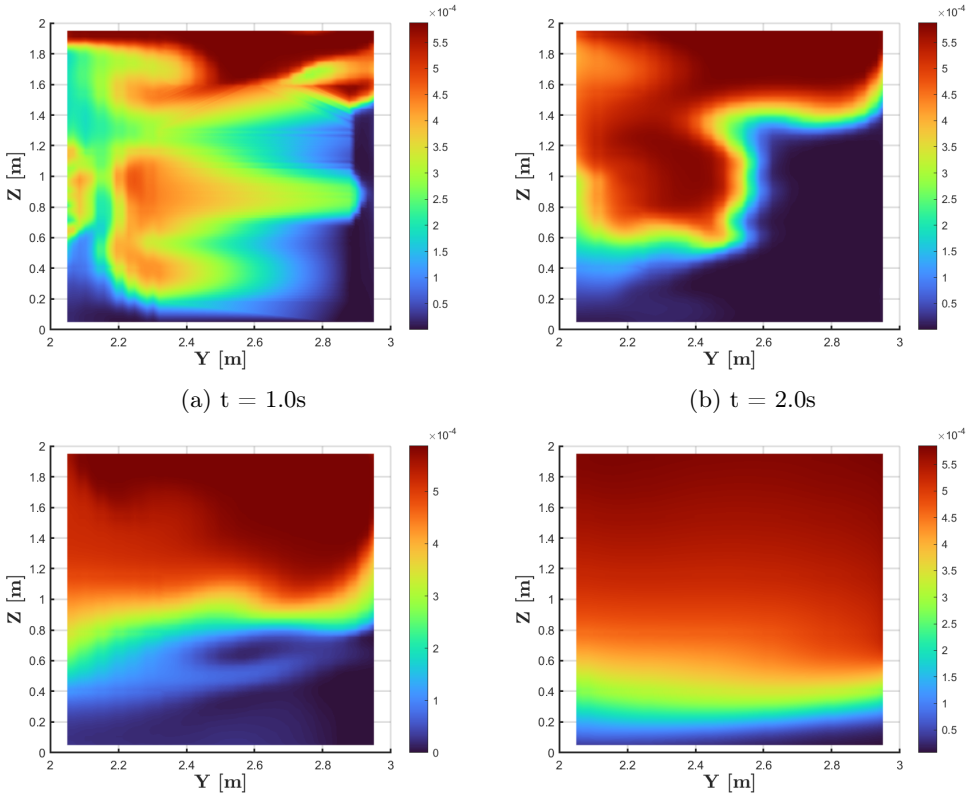

(a) t = 1.0s (b) t = 2.0s

(c) t = 3.0s (d) t = 4.0s

Figure 45: Mass fraction contours for hinged door

Contour plots showing the u-component velocity can be seen in figure 46. It is clear that positive velocity happens in the top half of the doorway, which matches with how we see SF_6 enter the inner zone. In figure 46d we see that the highest values can be found at the very edge, which could be explained by fluids entering and leaving the inner zone through the small gap between the door and the walls.

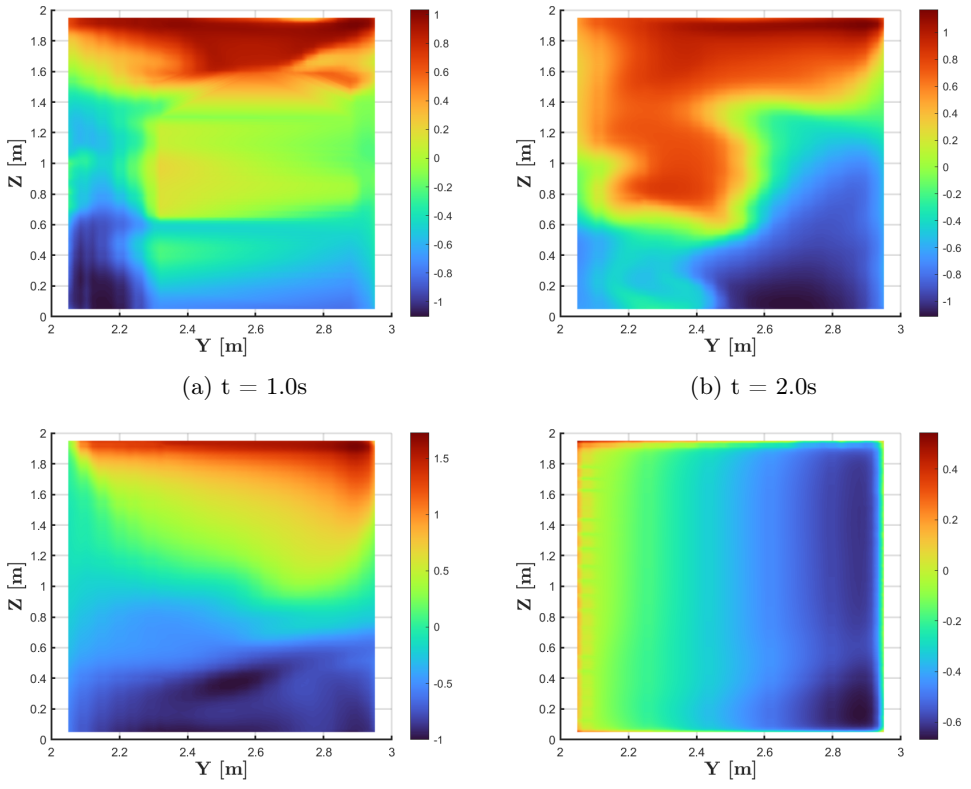

(a) t = 1.0s (b) t = 2.0s

(c) t = 3.0s (d) t = 4.0s

Figure 46: Velocity contours for hinged door

Figure 47 shows the 2D line plots for mass of SF_6 exchanged and average velocity through the doorway for the hinged door. In figure 47a we can read that the global maximum for mass of SF_6 transferred occurs right at the beginning of the simulation, with $3.46e^{-05}$kg exchanged and an air velocity of 0.38m/s. Another interesting observation is that the global minimum occurs right before the door closes again, with $-2.29e^{-05}$kg transferred and an air velocity of -0.32m/s. This is most likely the door pushing a relatively large amount of SF_6 out into the outer zone again. Otherwise a local minimum can be observed at t = 0.8s with $7.49e^{-08}$kg of SF_6 exchanged and an air velocity of -0.07m/s, and a local maximum at t = 2.0s with $3.10e^{-05}$kg of SF_6 exchanged and an air velocity of 0.08m/s. From t = 3.5s and onward there is a decrease of mass exchanged which lasts until the end of the simulation. Figure 47c presents the cumulative mass of SF_6 transferred throughout the hinged door simulation. Reading the graph we see that a total of 0.011kg of SF_6 has been transferred through the doorway. At the very end of this figure we see a small decrease in mass exchanged, which lines up well with what can be seen in figure 47a.

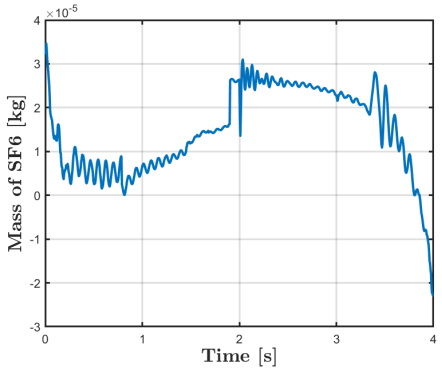

(a) Mass of SF_6 exchanged

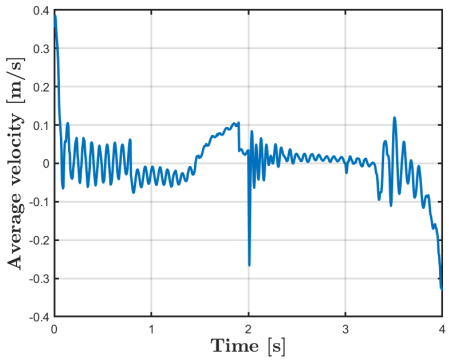

(b) Average velocity

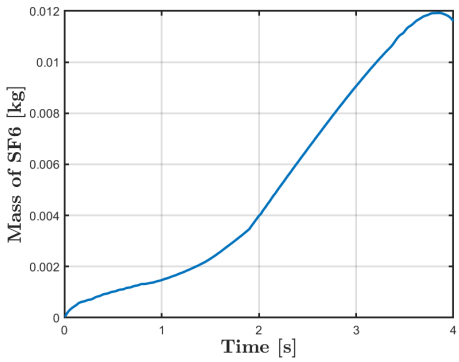

(c) Cumulative SF_6 for hinged door

Figure 47: 2D line plots showing mass transfer and velocity for hinged door

5.2.1 Thermal results

In figure 48 we see the scalar fields showing temperature exchange. Both figure 48b and 48c depicts mixing layers in the doorway. These figures along with figure 48d show small plumes of heat follow the moving person into the inner zone. From this figure we can also observe that the temperature around the door in the inner zone has increased. The same "tongue" that we saw in figure 44a is also present here. Compared to the images for the sliding door the change in temperature is more noticeable here.

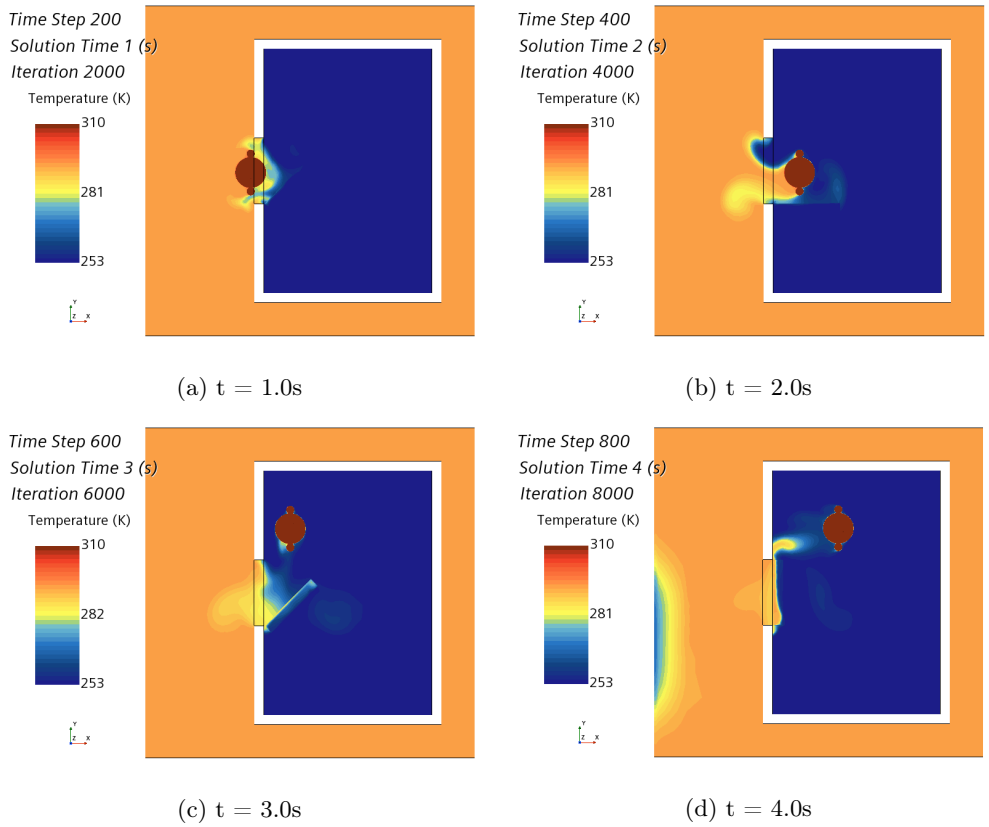

(a) t = 1.0s (b) t = 2.0s

(c) t = 3.0s (d) t = 4.0s

Figure 48: Scalar fields for hinged door with $\Delta T = 40°C$

Contour plots showing temperature contours can be seen in figure 49. Like could be observed in the plots for SF_6, mixing layers at the beginning of the simulation are to be found all across the doorway. Figure 49c clearly shows warm SF_6 enter through the top half and cold air leave through the bottom half of the doorway.

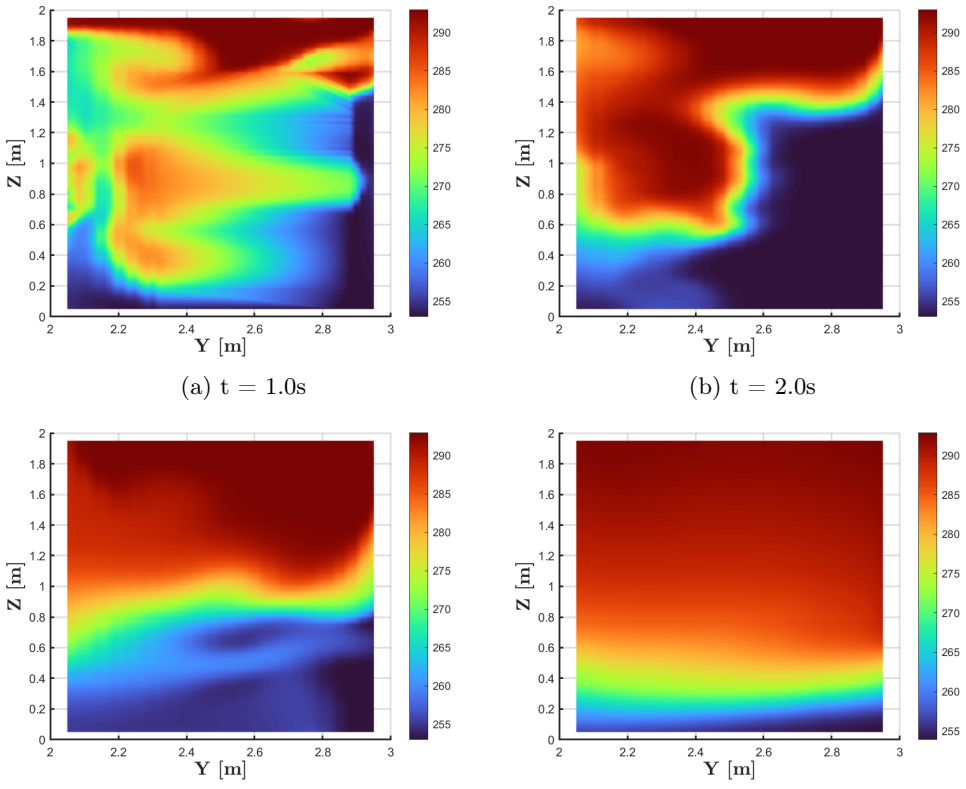

(a) t = 1.0s (b) t = 2.0s

(c) t = 3.0s (d) t = 4.0s

Figure 49: Temperature contours for hinged door

Figure 50 shows 2D line plots for energy transferred. From figure 50a we see that at the very start of the simulation 17.58kJ of energy was transferred, and at the very end -14.97kJ of energy was transferred. We have a local maximum at t = 3.5s with 5.47kJ of energy transferred, and a local minimum at t = 2.0s with -12.14kJ of energy transferred. Reading figure 50b we can see that a total of 3.65kJ was transferred. Note that the cumulative amount of energy transferred from t = 3.5s and to the end of the simulation drops drastically.

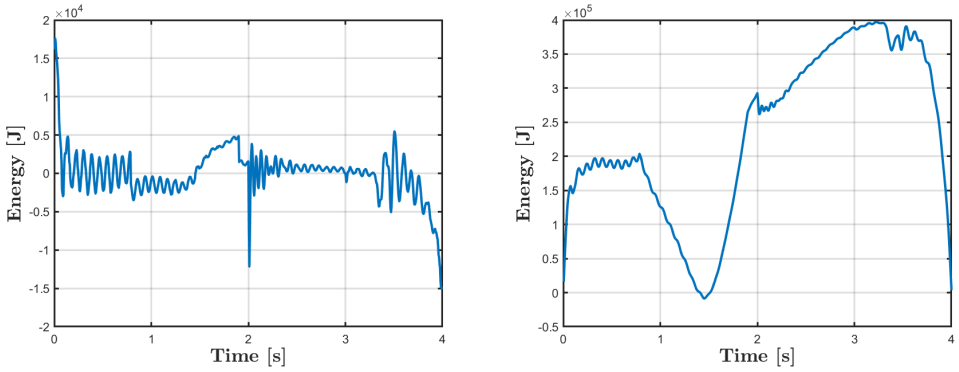

(a) Energy transferred (b) Cumulative energy transferred

Figure 50: 2D line plots for hinged door showing energy transfer

5.3 Results for double sliding doors

For the case of the double sliding door the simulation yielded unexpected results. The residuals in Star-CCM+ show some unusually high spikes in both turbulent dissipation rate and turbulent kinetic energy towards the end of the simulation (see appendix B.1). In addition to this, the thermal analysis also showed some unexpected results. It was decided that the final 0.25s of the simulation would not be included in this thesis. The results leading up to this time have been included in this thesis for completion's sake, but will require further testing before they can be considered valid.

Figure 51 depicts the scalar and vector fields for the double sliding doors while the doors are opening. There is little information to gather from figure 51a but in figure 51c we can see that there is both SF_6 entering through the top half and air leaving through the bottom half of the doorway. Figure 51b shows that the highest air velocity can be found between the opening doors. Compared to the two previous simulations this is more similar to the single sliding door.

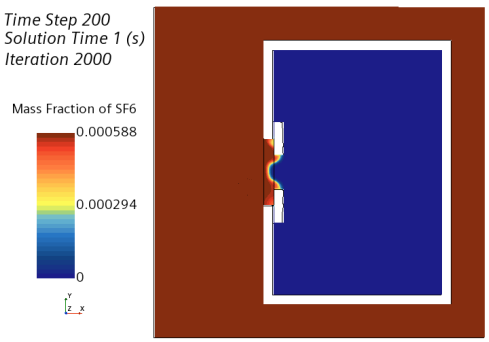

(a) Scalar field, top view

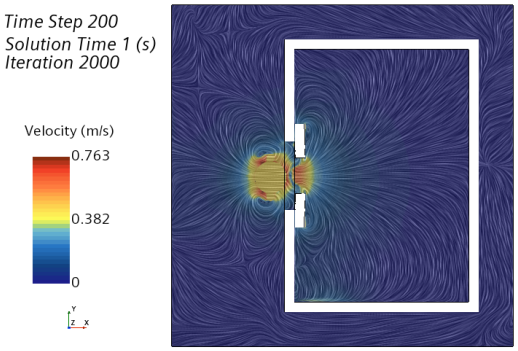

(b) Vector field, top view

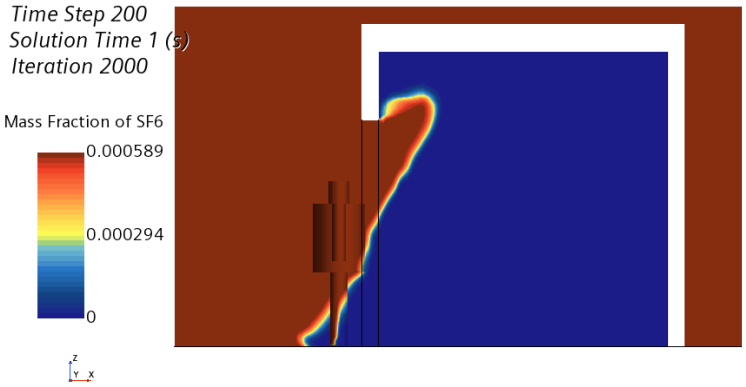

(c) Scalar field, side view

Figure 51: Double doors when opening at t = 1.0s

In figure 52 we see the scalar and vector fields for when the double sliding doors are fully opened. It is clear from figure 52c that a plume of SF_6 have entered the inner zone. We can also see air flowing out through the bottom half of the doorway. Here a mixing layer in the outer zone is also more evident. Figure 52b illustrates that the air velocity in is highest between the gap between the moving doors and the moving person.

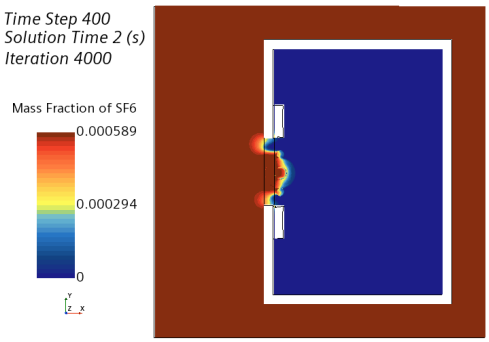

(a) Scalar field, top view

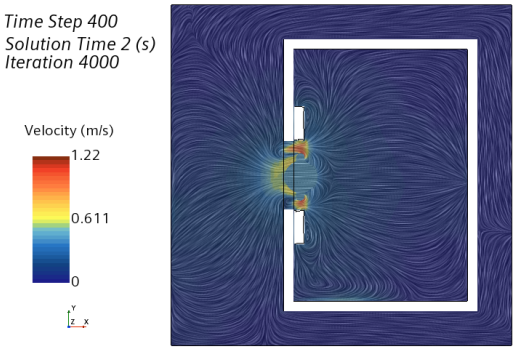

(b) Vector field, top view

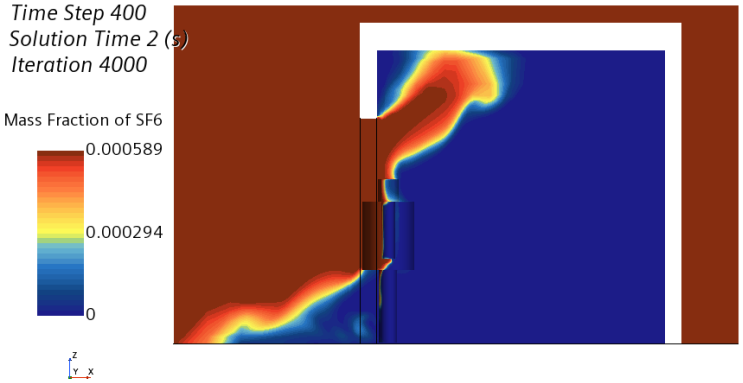

(c) Scalar field, side view

Figure 52: Double doors when fully opened at t = 2.0s

Figure 53 depicts the scalar and vector fields for when the double sliding doors are closing. From figure 53c it can be seen that a significant amount of SF_6 has now entered the inner zone and is starting to settle along the ceiling. Figure 53a shows the mixing layers in the outer zone and by the ceiling in the inner zone grow in width. It can also be observed that the gas entering in the wake of the moving person is seemingly clinging to them. This is confirmed by figure 53b where it can be seen that the air velocity around the moving person is still relatively high. Comparing these images to the two previous simulations, it is clear that this simulation still resembles the single sliding door the most.

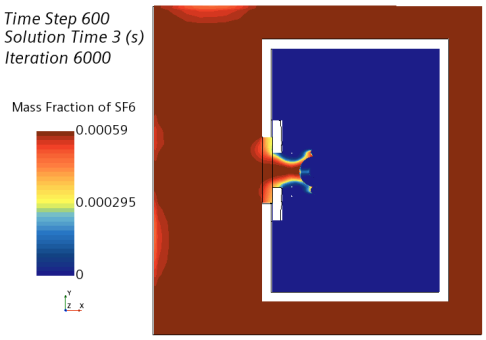

(a) Scalar field, top view

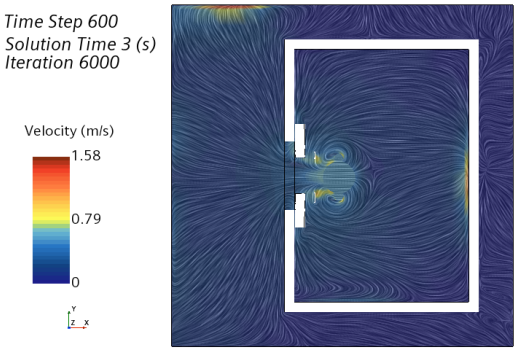

(b) Vector field, top view

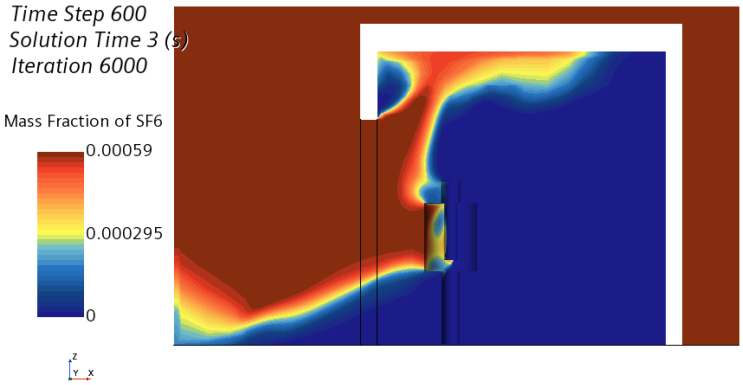

(c) Scalar field, side view

Figure 53: Double doors when closing at t = 3.0s

Figure 54 shows the scalar and vector fields for when the double sliding doors are almost entirely closed. Figure 54a illustrates a cloud of SF_6 following in the wake of the moving person. In figure 54c we can see the presence of SF_6 in the inner zone, and that it is gathering towards the ceiling. We can also observe the presence of air in the outer zone. In both the inner and the outer zone mixing layers are clearly visible. Figure 54b shows vorticity concentrated around the moving person. There is also some observable activity in the outer zone.

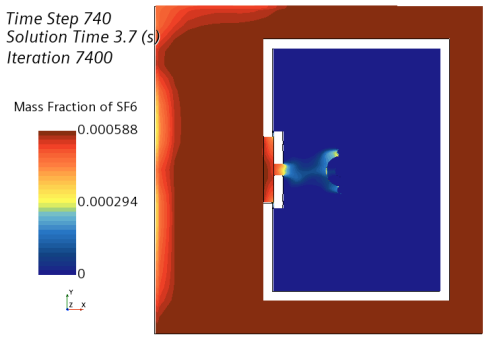

(a) Scalar field, top view

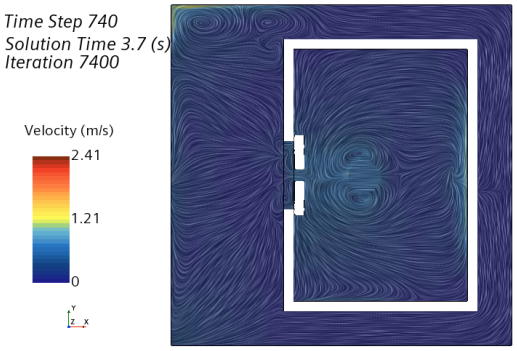

(b) Vector field, top view

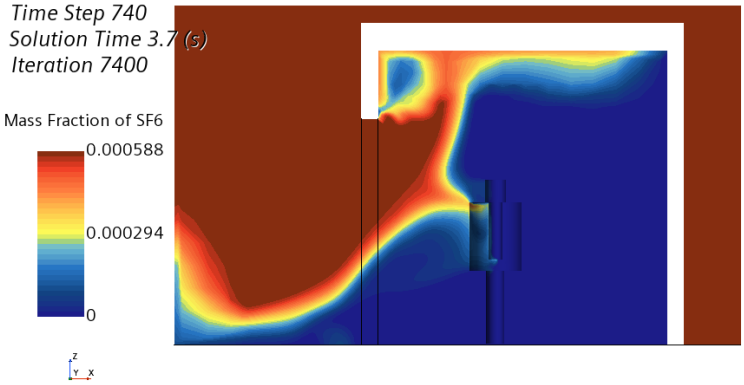

(c) Scalar field, side view

Figure 54: Double doors when closing at t = 3.7s

Contour plots showing mass fraction of SF_6 can be seen in figure 55. These figures clearly show air leaving the inner zone through the opening left by the moving doors. In figure 55b it is interesting to see the outline of the moving person, and how they drag SF_6 in with them. Figure 55d shows air mainly leaving the inner zone through the small gaps between the closing doors. We can also observe small areas around the lower edges where air is escaping.

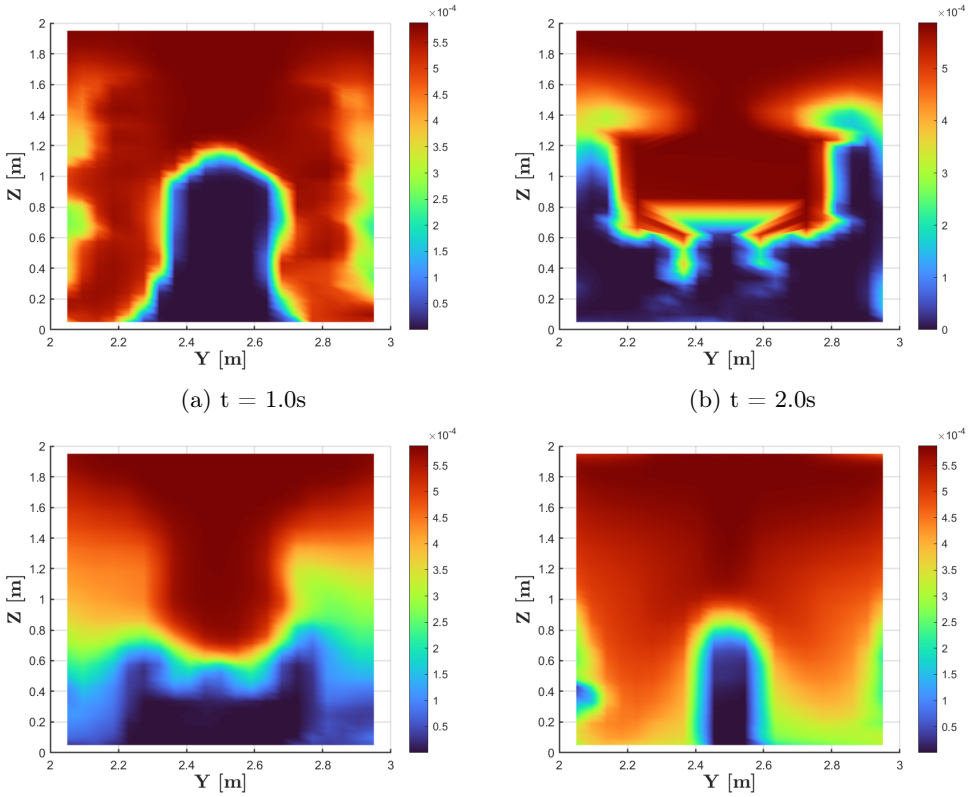

(a) t = 1.0s (b) t = 2.0s

(c) t = 3.0s (d) t = 3.7s

Figure 55: Mass fraction contours for double doors

Figure 56 depicts contour plots for the u-component for the double sliding doors. Initially we see the velocities match up well with what we saw in figure 55. We also get the nice outline of the moving person in figure 56b. In figure 56d most of the air movement is concentrated in the very middle of the doorway.

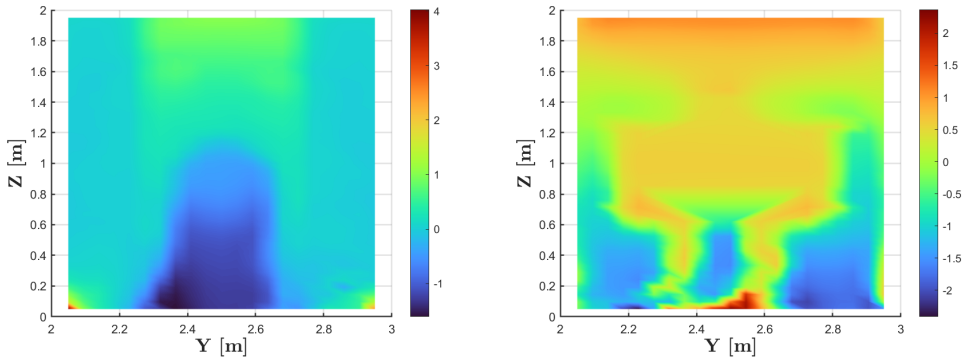

(a) t = 1.0s

(b) t = 2.0s

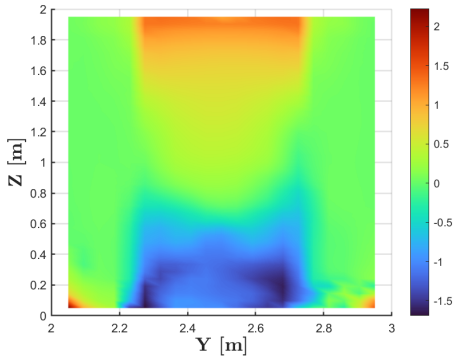

(c) t = 3.0s

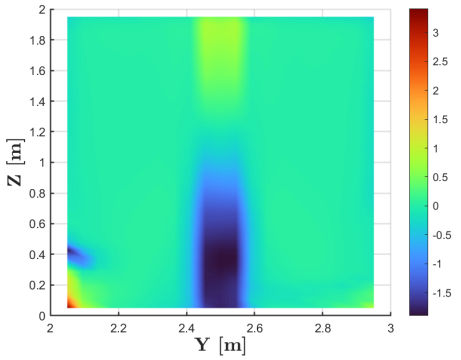

(d) t = 3.7s

Figure 56: Velocity contours for double doors

In figure 57 we see the 2D line plots for mass of SF_6 exchanged and the average velocity through the doorway. From figure 57a it can be seen that the maximum and minimum amounts of SF_6 transferred was $5.75e^{-06}$kg and $-1.76e^{-06}$kg respectively. Figure 57b tells us that the global maximum velocity occurs at t $\approx$ 2.6s with a value of 0.029m/s and the global minimum velocity occurs at t $\approx$ 3.7s with a value of -0.051m/s. From figure 57c we see that a total of 0.0016kg of SF_6 entered the inner zone.

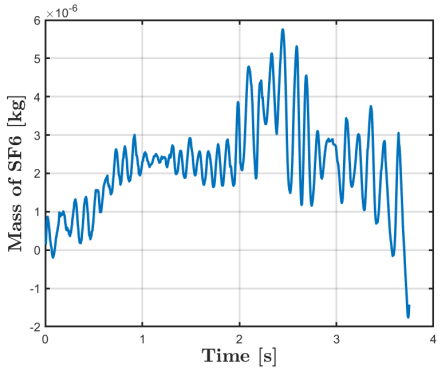

(a) Mass of SF_6 exchanged

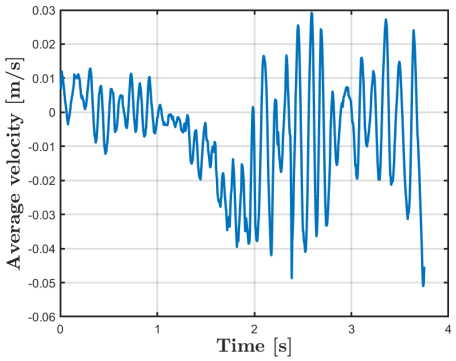

(b) Average velocity

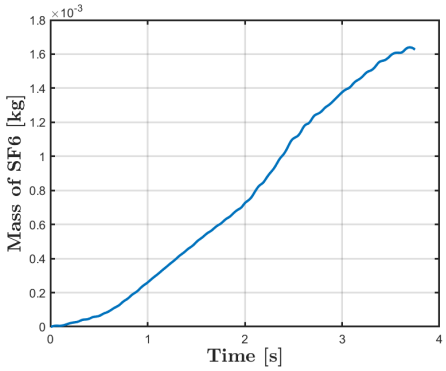

(c) Cumulative SF_6 for double doors

Figure 57: 2D line plots showing mass transfer and velocity for double doors

5.3.1 Thermal results

The scalar fields showing temperature for the double sliding doors are shown in figure 58. These figures line up well with what we saw in the scalar fields showing mass fraction of SF_6. The warm air of the outer zone enters with the movement of the person, being dragged in their wake. At the end of the simulation we can see a plume around the human body. Compared to the two previous studies, these images also more resemble the single sliding door ones.

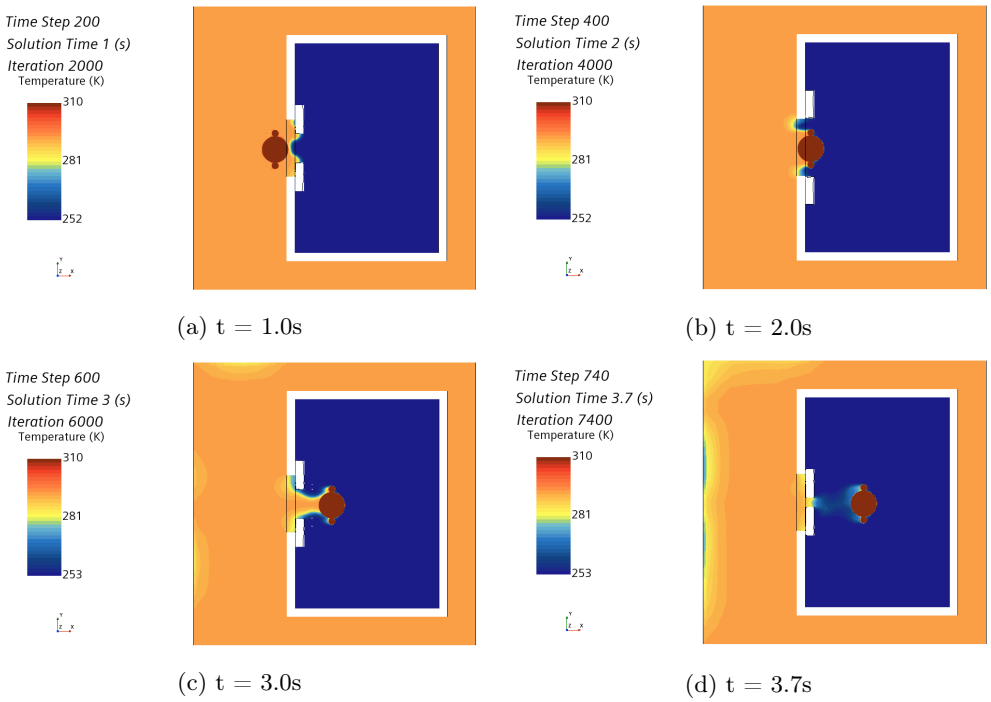

(a) t = 1.0s (b) t = 2.0s

(c) t = 3.0s (d) t = 3.7s

Figure 58: Scalar fields for double doors with $\Delta T = 40°C$

Figure 59 show contour plots for the double doors, showing temperature contours. It is clear that for the first three seconds of simulation, these images match with what we saw for mass fraction of SF6 transferred and average velocity. In figure 59d we see that cold air leaving the inner zone is now concentrated in the very middle of the doorway.

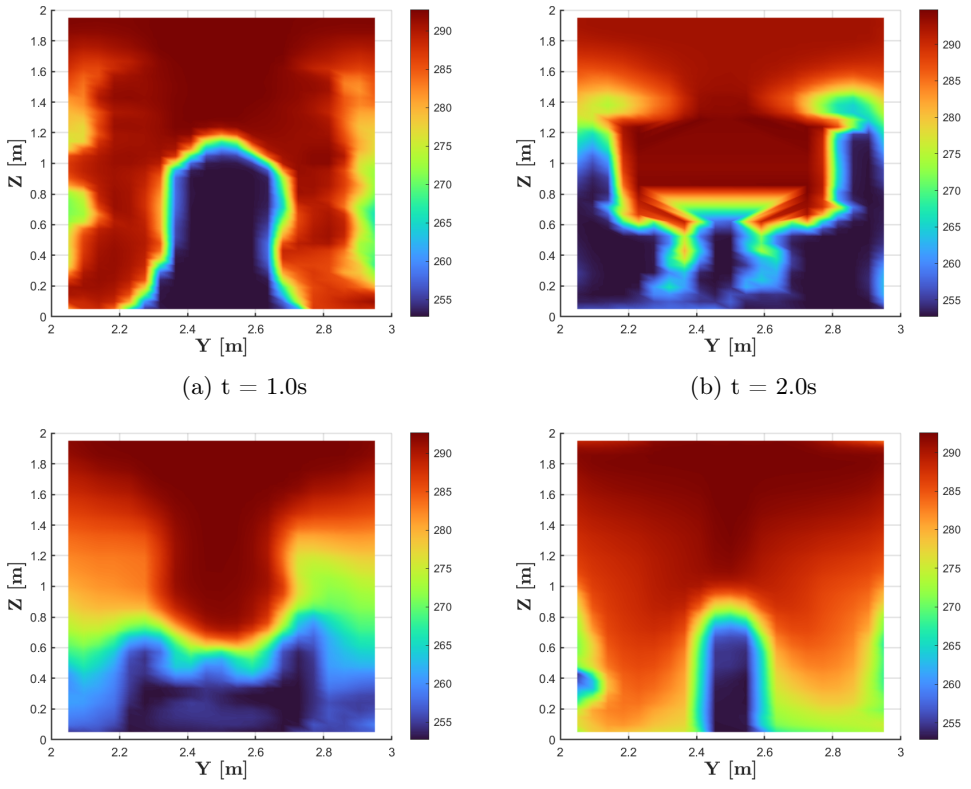

(a) t = 1.0s (b) t = 2.0s

(c) t = 3.0s (d) t = 3.7s

Figure 59: Temperature contours for double doors

In figure 60 we see the graphs showing energy transfer for the double sliding doors. From figure 60a it can be seen that at t ≈ 2.6s at most 1.33kJ , and at t ≈ 3.7s at least -2.31kJ of energy was transferred. Figure 60b tells us that a total of -210.00kJ of energy was transferred.

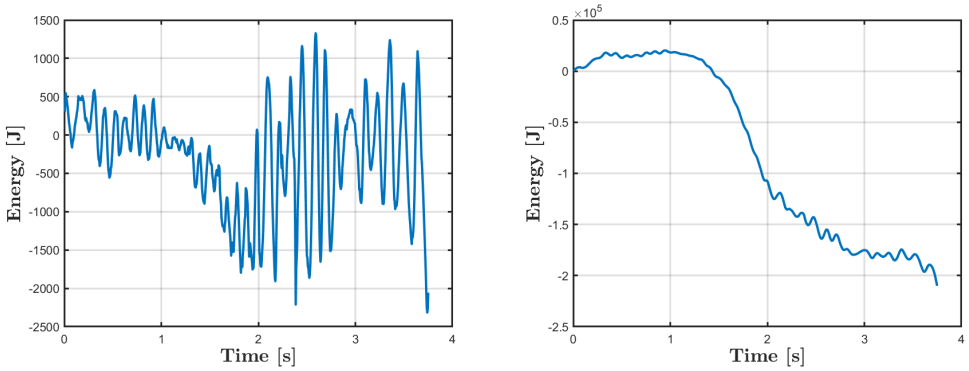

(a) Energy transferred (b) Cumulative energy transferred

Figure 60: 2D line plots for double sliding doors showing energy transfer

5.4 Summary of results

In this section the results from all three simulations are compared. The comparisons for total mass SF_6 and energy transferred are presented in table 11.

Table 11: Comparison of case simulations

Door type	Total mass SF_6 transferred [kg]	Total energy transferred [kJ]
Sliding	0.010	917
Hinged	0.011	3.65
Double sliding	0.0016	-210

From this table we see that the hinged door simulation transferred the most amount of SF_6, and that the double sliding doors transferred the least amount of SF_6. We see that the single sliding door had the most energy transferred *into* the inner zone, while the double sliding doors had the most energy transferred *from* the inner zone. For residuals from all three simulations see appendix B.1. For run time of each simulation, see appendix E

5.5 Discussion

The preliminary results for the single sliding door showed little mass exchange throughout the simulation. That the door moves parallel to the wall appears to create a minimal vorticity capable of dragging tracer gas into the inner zone. This door had comparatively small amounts of SF_6 gas enter the inner zone, which has also been shown in previous studies. Figure 33b from this simulation showed high air velocities in the gaps between the walls and the door, and the door and the person. One possible cause for this could be that the CFD model had not been properly defined for such small gaps. This type of door had the most energy transferred into the inner zone by a significant margin. It could be that this is because the movement of the door is doing little to influence the air velocity in the doorway while the moving person, moving perpendicular to the door, is capable of generating a much larger flow into the inner zone. This matches with what we saw in figure 40b, where very little energy was transferred in the first second of simulation. It isn't until the moving person enters the doorway that we start seeing activity.

For the hinged door the preliminary results showed high turbulence. Compared to the other two simulations, the motion of this type of door generates greater vorticity both around the door itself and inside the zone into which it is moving. As was the case in the validation case, this type of door has the largest amount of SF_6 transferred, which is corresponds with previous similar studies. What is interesting however is that not much energy was transferred, indicating that this type of door is well suited to transferring mass. One possibility is that the movement of the two moving solids had a canceling effect on each other, leading to less turbulence in the doorway. In figure 50b we also see a sharp drop in energy transfer towards the end of the simulation, meaning that the door is "pushing" the energy out.

From the preliminary results for the double sliding door it is evident that this type of doors have the least amount of SF_6 transferred into the inner zone. By inspecting figure 55 we can see that the doorway is covered in mixing layers from beginning to end of the simulation. When comparing air velocity in figure 57b to the two previous simulations, figure 37b and 47b, it is

clear that this model shows more chaotic and random behaviour. This is backed up by figure 56, where we can observe more mixing layers than in the other simulations. Unlike the two other simulations, this model showed negative energy transfer for most of the simulation time. One possible explanation for this behaviour is that the opposite motion of the double doors is ideal for creating vorticity capable of dragging cold air out of the inner zone.

6 Conclusion

In this thesis transient mass and heat exchange through a doorway was analysed. Three different cases were investigated, one for each of the three type of doors. In addition to this, a person moving through the doorway was included in each model. The unsteady fluid flow physics involves a multi-component gaseous system, with the doors and the person being treated as moving solids. An overset mesh was applied to the solid bodies movement in two initially separated areas, one containing air and one containing SF_6 gas. The 3D compressible multi-component fluid flow was solved using Reynolds Averaged Navier-Stoked equations and $k - \epsilon$ turbulence model. The simulation time for each model was set to run until physical time reached four seconds. During this time, the door is set to open during the first two seconds, and close during the last two seconds. Each simulation file was submitted to the super-computer cluster Fram, courtesy of UiT - Arctic University of Norway. The flow dynamics of each case model have been presented and analysed qualitatively using scalar fields showing SF_6 and temperature distribution, and vector fields using line integrated convolution. In addition to these figures, a presentation grid was defined in the doorway which collected data that was then post-processed in MATLAB to produce 2D line plots and Delaunay triangulation plots which were analysed quantitatively.

The preliminary findings showed that the hinged type door had the highest vorticity, and the highest cumulative mass of SF_6 transferred. Corroborating with previous studies, the hinged type door is associated with having the most complex fluid flow patterns. Furthermore, the findings showed that the sliding door had the most energy transferred *into* the inner zone while the double sliding doors had the most energy transferred *out from* the inner zone. Some unexpected results showed up for the last 0.25s of the double sliding door simulation. These were omitted from this work, as they were considered to be non-valid.

The analysis done in this thesis highlights the importance of having a properly defined CFD model in order to get valid results. It also shows that CFD software is a powerful tool when analysis indoor climate. To the best of the authors knowledge there is little literature investigating the detailed numerical analysis of the effects double sliding doors have on transient flow across doorways, so this work adds to the pool of knowledge that future studies can build their work from.

6.1 Future work

This work forms a basis for further detailed analysis of different indoor environment conditions. An experimental model using different type of doors and a mannequin moving through the door-opening could be performed to verify the numerical results. Similar numerical models could be run with altered parameters, such as introducing a pressure difference between the separated zones. Another altercation would be to increase the physical time of the simulation in order to achieve better thermal analyses. A larger scale model could be designed, which would highlight the turbulence scales in simulations like these. Numerical models with internal gains, such as a ventilation system or a cooling fan, could also be explored. There is also the possibility of improving upon the model human by introducing oscillating movement of arms and legs.

References

[1] S. Tian, Y. Gao, S. Shao, H. Xu, and C. Tian, "An experimental investigation of the single-sided infiltration through doorways of the cold store," *International journal of refrigeration*, vol. 73, pp. 175–182, 2017.

[2] L. Chang, X. Zhang, S. Wang, and J. Gao, "Control room contaminant inleakage produced by door opening and closing: Dynamic simulation and experiments," *Building and environment*, vol. 98, pp. 11–20, 2016.

[3] L. Fontana and A. Quintino, "Experimental analysis of the transport of airborne contaminants between adjacent rooms at different pressure due to the door opening," *Building and environment*, vol. 81, pp. 81–91, 2014.

[4] J. Hendiger, M. Chludzińska, and P. Zietek, "Influence of the pressure difference and door swing on heavy contaminants migration between rooms," *PloS one*, vol. 11, no. 5, pp. e0 155 159–e0 155 159, 2016.

[5] X. Shao, K. Hashimoto, L. Fang, A. K. Melikov, K. G. Naydenov, and C. Rasmuseen, "Experimental study of airborne particle transmission through the doorway of a cleanroom due to the movement of a person," *Building and environment*, vol. 183, p. 107205, 2020.

[6] A. Ayarmal, O. Melhus, and A. Chaudhuri, "The effects of fan and door opening on a cold storage room: a numerical study," *Linköping Electronic Conference Proceedings*, 2018.

[7] J. Gonçalves, J. Costa, and A. Lopes, "Analysis of the air infiltration through the doorway of a refrigerated room using different approaches," *Applied thermal engineering*, vol. 159, p. 113927, 2019.

[8] L. Wang, L. Zhang, and G. Lian, "A cfd simulation of 3d air flow and temperature variation in refrigeration cabinet," *Procedia engineering*, vol. 102, pp. 1599–1611, 2015.

[9] S. Tian, Y. Gao, S. Shao, H. Xu, and C. Tian, "Numerical investigation on the buoyancy-driven infiltration airflow through the opening of the cold store," *Applied thermal engineering*, vol. 121, pp. 701–711, 2017.

[10] X. Zhang, J. Han, J. Qian, Y. Wang, L. Wang, and X. Yang, "Computational fluid dynamic study of thermal effects of open doors of refrigerated vehicles," *Journal of food process engineering*, vol. 41, no. 3, pp. e12 662–n/a, 2018.

[11] B. Zhou, L. Ding, F. Li, K. Xue, P. V. Nielsen, and Y. Xu, "Influence of opening and closing process of sliding door on interface airflow characteristic in operating room," *Building and environment*, vol. 144, pp. 459–473, 2018.

[12] P. Kalliomäki, K. Hagström, H. Itkonen, I. Grönvall, and H. Koskela, "Effectiveness of directional airflow in reducing containment failures in hospital isolation rooms generated by door opening," *Building and environment*, vol. 158, pp. 83–93, 2019.

[13] E. S. Mousavi, R. Jafarifiroozabadi, S. Bayramzadeh, A. Joseph, and D. San, "An observational study of door motion in operating rooms," *Building and environment*, vol. 144, pp. 502–507, 2018.

[14] A. Bhattacharya, A. R. Metcalf, A. M. Nafchi, and E. S. Mousavi, "Particle dispersion in a cleanroom - effects of pressurization, door opening and traffic flow," *Building research and information : the international journal of research, development and demonstration*, vol. 49, no. 3, pp. 294–307, 2021.

[15] A. Hathway, I. Papakonstantis, A. Bruce-Konuah, and W. Brevis, "Experimental and modelling investigations of air exchange and infection transfer due to hinged-door motion in office and hospital settings," *The International journal of ventilation*, vol. 14, no. 2, pp. 127–140, 2015.

[16] P. Kalliomäki, P. Saarinen, J. W. Tang, and H. Koskela, "Airflow patterns through single hinged and sliding doors in hospital isolation rooms – effect of ventilation, flow differential and passage," *Building and environment*, vol. 107, pp. 154–168, 2016.

[17] A. Bhattacharya, A. Ghahramani, and E. Mousavi, "The effect of door opening on air-mixing in a positively pressurized room: Implications for operating room air management during the covid outbreak," *Journal of Building Engineering*, vol. 44, p. 102900, 2021.

[18] S. Lee, B. Park, and T. Kurabuchi, "Numerical evaluation of influence of door opening on interzonal air exchange," *Building and environment*, vol. 102, pp. 230–242, 2016.

[19] R. Carneiro, P. Gaspar, and P. Silva, "3d and transient numerical modelling of door opening and closing processes and its influence on thermal performance of cold rooms," *Applied thermal engineering*, vol. 113, pp. 585–600, 2017.

[20] S. Tian, Y. Gao, S. Shao, H. Xu, and C. Tian, "Development of an unsteady analytical model for predicting infiltration flow rate through the doorway of refrigerated rooms," *Applied thermal engineering*, vol. 129, pp. 179–186, 2018.

[21] Siemens Digital Industries Software, "Simcenter STAR-CCM+, version 2022.1," Siemens 2022.

[22] F. Hermansen, "Transient flow analysis of opening hinged/sliding door," 2021. [Online]. Available: https://hdl.handle.net/11250/2772543

[23] H. Versteeg, "An introduction to computational fluid dynamics : the finite volume method," Harlow, 2007.

[24] Y. A. Çengel, "Fluid mechanics : fundamentals and applications," New York, NY, 2018.

[25] *MATLAB version 9.9.0.1570001 (R2020b) Update 4*, The Mathworks, Inc., Natick, Massachusetts, 2020.

[26] U. A. U. of Norway. Fram documentation. [Online]. Available: https://documentation.sigma2.no/hpc_machines/fram.html

List of Figures

List of Tables

A Supercomputer submission file

sbatch_star (15) – Notisblokk

Fil Rediger Format Vis Hjelp

```
#!/bin/bash
# Job name:
#SBATCH --job-name=starp3
#SBATCH --mem=100G
#
# Project:
#SBATCH --account=nn8005k
#
# Wall clock limit:
#SBATCH --mail-user=s326356@oslomet.no
#SBATCH --mail-type=END
#SBATCH --partition=bigmem

# Number of tasks (cores):
#SBATCH --nodes=3 --ntasks-per-node=32

# Max memory usage per task:
####SBATCH --mem-per-cpu=4G

#SBATCH --time=10:00:00

## Set up job environment:
####source /cluster/bin/jobsetup
set -o errexit # exit on errors
set -o nounset # Treat unset variables as errors
module --force purge

submissionfolder='ThermalHinged'
simfile='ThermalHinged.sim'

mystar='/cluster/projects/nn8005k/STAR/17.02.007-R8/STAR-CCM+17.02.007-R8/star/bin/starccm+'
mypod='riVTbnNk1cqvMetK3BDCJA'

## Set up input and output files:
tar -cvf temp.tar $submissionfolder/
mv temp.tar $SCRATCH

cd $SCRATCH
tar -xvf temp.tar
cd $submissionfolder/


$mystar -np $SLURM_NPROCS -power -podkey $mypod -licpath 1999@flex.cd-adapco.com -batch $simfile

rsync -arv  $SCRATCH/$submissionfolder  /cluster/projects/nn8005k/Fredrik/RES/

exit 0
```

Figure 61: File used for submitting jobs to supercomputer cluster Fram

B Residuals

B.1 Case model residuals

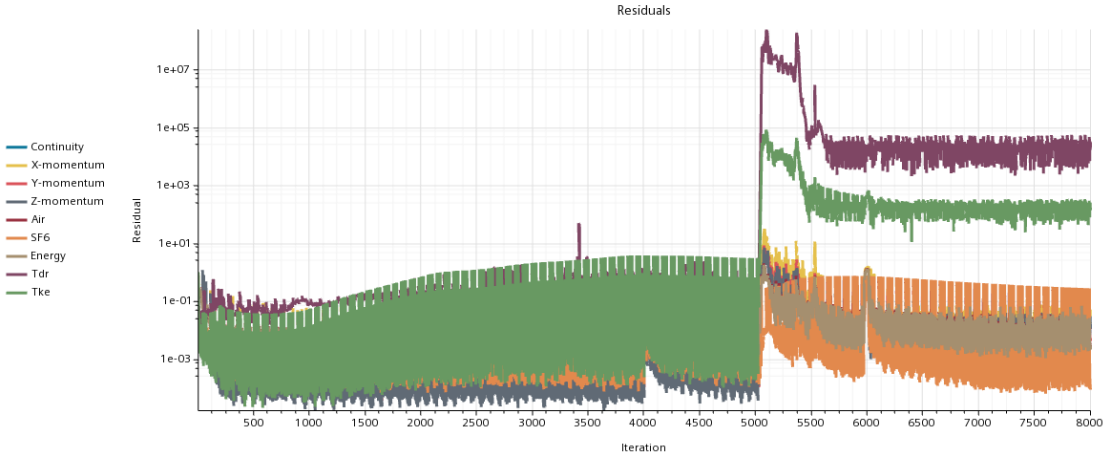

Figure 62: Residuals for sliding door

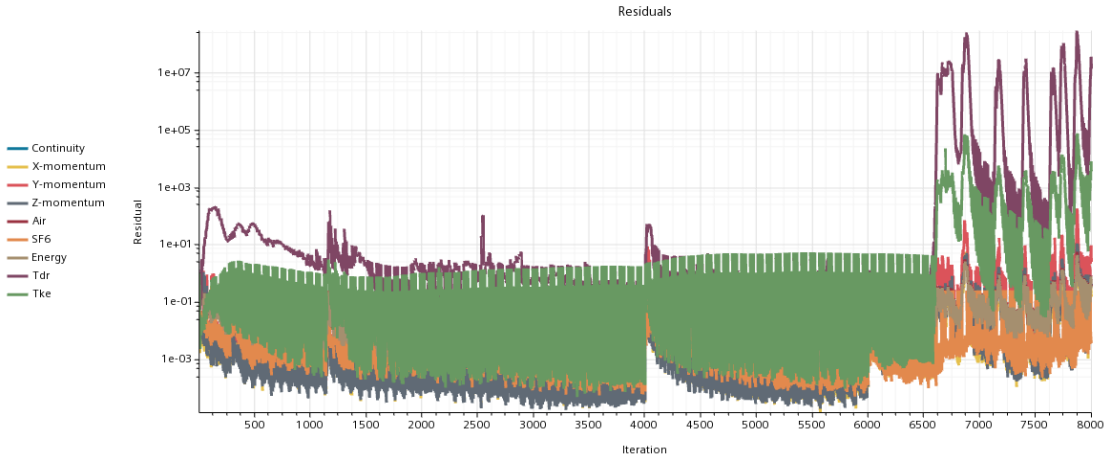

Figure 63: Residuals for hinged door

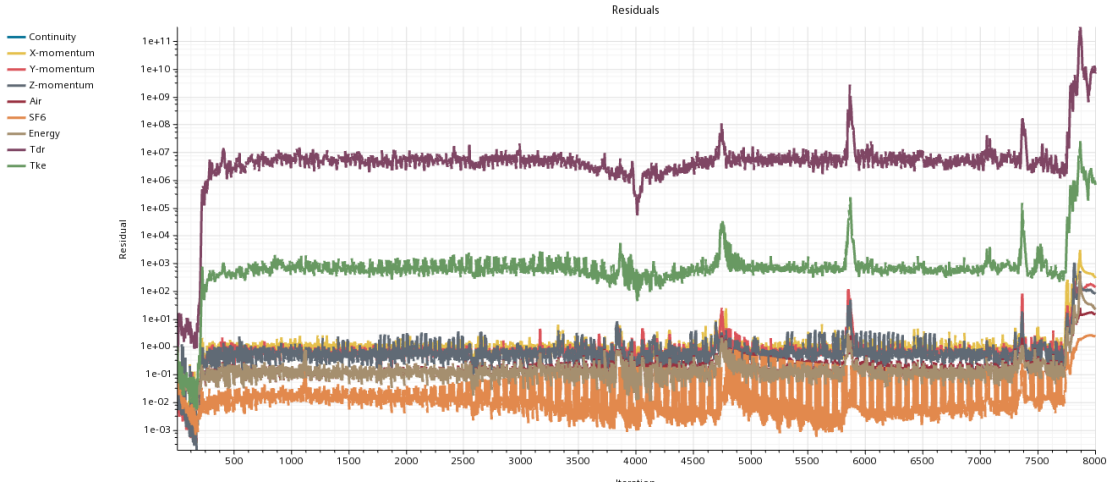

Figure 64: Residuals for double doors

B.2 Verification model residuals

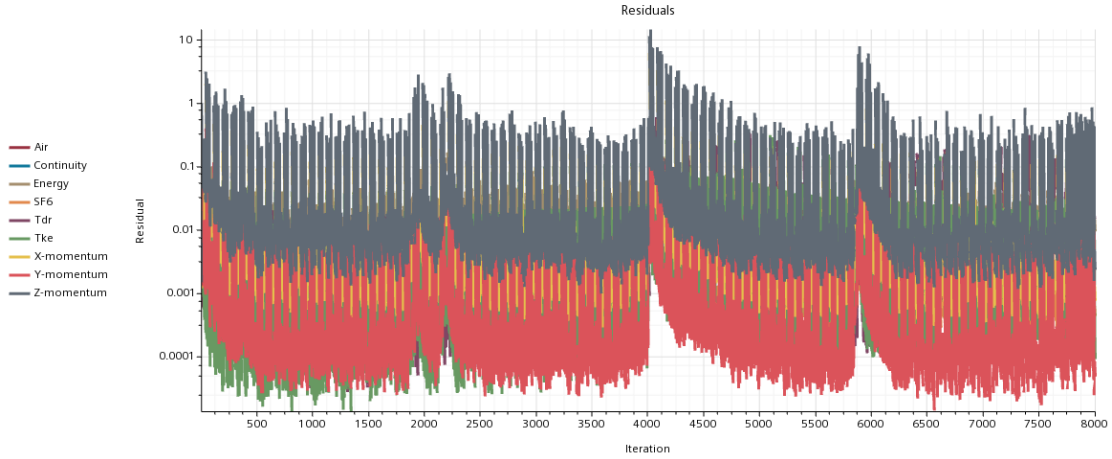

Figure 65: Residuals for sliding door

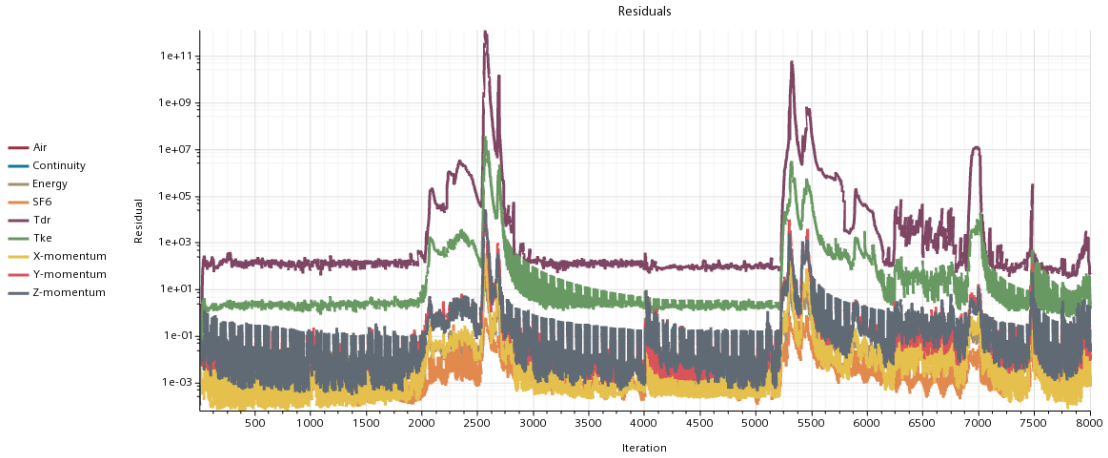

Figure 66: Residuals for hinged door

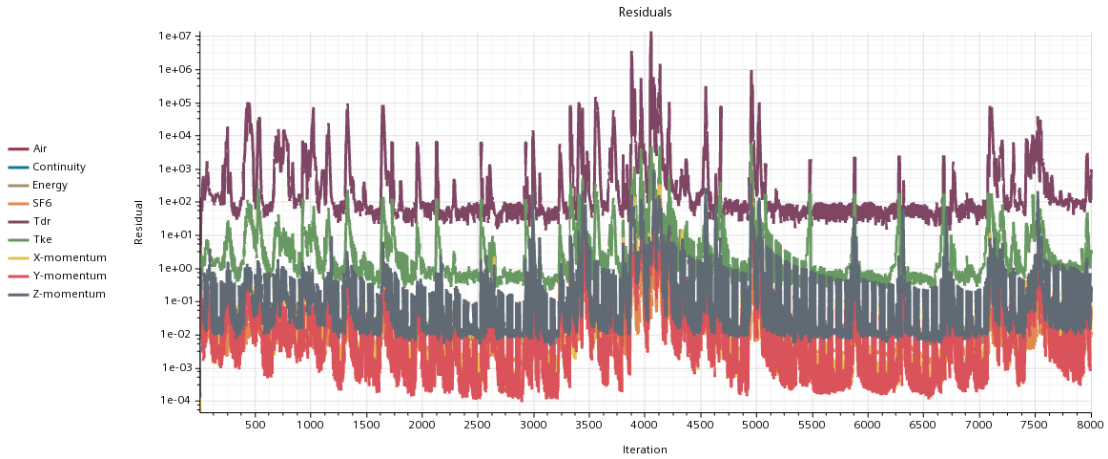

Figure 67: Residuals for double door

C MATLAB scripts

```
clear all;
close all;
clc;

dt = 0.005;      % time step [s]
dx = 0.05;       % length of presentation grid [m]
dy = 0.05;       % length of presentation grid [m]
A = dx * dy;     % area of presentation grid [m^2]
cp = 1003.5;     % specific heat capacity [J/kg*K]

n = 800;         % total number of files
m = n;           % length of array

M = zeros(m,1); % array for mass
E = zeros(m,1); % array for energy
V = zeros(m,1); % array for velocity
part1 = 'slidingtable/XYZ_Internal_Table_table_';
part3 = '.csv';
count = 1;

for i = 1:n      % for-loop
    part2 = num2str(i,'%d');
    filename = [part1 part2 part3]
    Data = readtable(filename);
    mydata = table2array(Data);
    mdot = A * mydata(:,2) .* mydata(:,3) .* mydata(:,9);
    totalm = mdot * dt;
    edot = A * cp * mydata(:,3) .* mydata(:,8) .* mydata(:,9);
    totale = edot * dt;
    v_avg = A * mydata(:,9)
    M(count) = sum(totalm);
    E(count) = sum(totale);
    V(count) = sum(v_avg) / (A * 5151);
    count = count + 1;
end

figure           % mass transferred
plot(M,'LineWidth',2.0);
set(gca,'XTick',[0:200:800])
set(gca,'XTickLabel',[0:4])
xlabel('\fontsize{14},\textbf{Time [s]}','Interpreter','latex')
ylabel('\fontsize{14},\textbf{Mass of SF6 [kg]}','Interpreter','latex')
ax = gca;
ax.LineWidth = 1.5;
grid on
saveas (gcf,'model/sliding/sliding_sf6.png')
```

Figure 68: Example of MATLAB script for 2D line plots

```
clear all;
close all;
clc;

n = 800;          % number of files
cp = 1003.5;      % specific heat capacity [J/kg*K]

part1 = 'slidingtable/XYZ_Internal_Table_table_';
part2 = num2str(n,'%d');
part3 = '.csv';
filename = [part1 part2 part3];
Data = readtable(filename);
mydata = table2array(Data);

tri = delaunay([mydata(:,11), mydata(:,12)]);

% Mass fraction of SF6
figure
h = trisurf(tri, mydata(:,11), mydata(:,12), mydata(:,2));
view([0,90])
colormap turbo
shading interp
colorbar EastOutside
xlabel('\fontsize{14},\textbf{Y [m]}','Interpreter','latex')
ylabel('\fontsize{14},\textbf{Z [m]}','Interpreter','latex')
ax = gca;
ax.LineWidth = 1.2;
grid on
saveas (gcf,'model/sliding/sliding_delaunay_sf6_4s.png')

% u component of velocity
figure
h = trisurf(tri, mydata(:,11), mydata(:,12), mydata(:,9));
view([0,90])
colormap turbo
shading interp
colorbar EastOutside
xlabel('\fontsize{14},\textbf{Y [m]}','Interpreter','latex')
ylabel('\fontsize{14},\textbf{Z [m]}','Interpreter','latex')
ax = gca;
ax.LineWidth = 1.2;
grid on
saveas (gcf,'model/sliding/sliding_delaunay_velocity_4s.png')
```

Figure 69: Example of MATLAB script for Delaunay triangulation

D .cvs tables

Column1	Column2	Column3	Column4	Column5	Column6	Column7	Column8	Column9	Column10	Column11	Column12
Density (kg/m^3)	Mass Fraction of SF6	Velocity[i] (m/s)	Pressure (Pa)	Temperature (K)	Area: Magnitude (m^2)	Position[X] (m)	Position[Y] (m)	Position[Z] (m)	X (m)	Y (m)	Z (m)
2.35444903373718	0.00058704812545329 3	-0.00343092414550483	101324.417619977	299.999725341797	1.79769313486232e+308	0.745	1.5764	0.43	0.745	1.5764	0.43
2.35445022583008	0.00058707158314064 1	-0.00278906733728945	101324.567398904	299.999816894531	1.79769313486232e+308	0.745	1.6108	0.43	0.745	1.6108	0.43
2.35445117950439	0.00058714568149298 4	-0.00215159077197313	101324.676609917	299.999877929688	1.79769313486232e+308	0.745	1.6452	0.43	0.745	1.6452	0.43
2.35445213317871	0.00058723666006699 2	-0.00149733433499932	101324.760010804	299.999908447266	1.79769313486232e+308	0.745	1.6796	0.43	0.745	1.6796	0.43
2.35445284843445	0.00058728241128847	-0.00118898798245937	101324.795421968	299.999877929688	1.79769313486232e+308	0.745	1.714	0.43	0.745	1.714	0.43
2.35445284843445	0.00058737036306411	-0.00062472635181620 7	101324.858571042	299.999938964844	1.79769313486232e+308	0.745	1.7484	0.43	0.745	1.7484	0.43
2.3544487953186	0.00058704253751784 6	-0.00353537243790925	101324.416540768	299.999755859375	1.79769313486232e+308	0.745	1.5764	0.468	0.745	1.5764	0.468
2.35444974899292	0.00058706739218905 6	-0.00284865265712142	101324.566279858	299.999847412109	1.79769313486232e+308	0.745	1.6108	0.468	0.745	1.6108	0.468
2.35445141792297	0.00058714189799502 5	-0.00218252534978092	101324.675409129	299.999847412109	1.79769313486232e+308	0.745	1.6452	0.468	0.745	1.6452	0.468
2.35445213317871	0.00058723433317605 56	-0.00152411567978561	101324.758984691	299.999908447266	1.79769313486232e+308	0.745	1.6796	0.468	0.745	1.6796	0.468
2.35445284843445	0.00058728142175823 5	-0.00120429556595703	101324.794569164	299.999877929688	1.79769313486232e+308	0.745	1.714	0.468	0.745	1.714	0.468
2.35445284843445	0.00058736983919516 2	-0.00060207020612731 6	101324.858006065	299.999938964844	1.79769313486232e+308	0.745	1.7484	0.468	0.745	1.7484	0.468
2.35444569587708	0.00058710365556180 5	-0.00532868783921003	101324.05349078	299.999603271484	1.79769313486232e+308	0.745	1.5076	0.506	0.745	1.5076	0.506
2.35444808006287	0.00058709264221548	0.00423350410373019	101324.320126317	299.999694824219	1.79769313486232e+308	0.745	1.542	0.506	0.745	1.542	0.506

Figure 70: .csv table for verification model, sliding door

Area: Magnitude (m^2)	Mass Fraction of SF6	Density (kg/m^3)	Pressure (Pa)	Position[X] (m)	Position[Y] (m)	Position[Z] (m)	Temperature (K)	Velocity[i] (m/s)	X (m)	Y (m)	Z (m)
1.79769313486232e+308	0.00058465122524685 9	2.41257230200539	101347.032685336	01.08.2022	2.392	1.627	292.781360815117	-0.0228876200412122	01.08.2022	2.392	1.627
1.79769313486232e+308	0.00058445668759783 1	2.41268263950802	101347.149135	01.08.2022	2.41	1.627	292.768089369903	-0.0244062825310449	01.08.2022	2.41	1.627
1.79769313486232e+308	0.00058433219171782 2	2.41275252935953	101347.219982851	01.08.2022	2.428	1.627	292.759655501303	-0.0252234696833373	01.08.2022	2.428	1.627
1.79769313486232e+308	0.00058434880236334 9	2.41274393566637	101347.241243336	01.08.2022	2.446	1.627	292.760751691118	-0.0248515043829659	01.08.2022	2.446	1.627
1.79769313486232e+308	0.00058434880236334 9	2.41274393566637	101347.241243336	01.08.2022	2.464	1.627	292.760751691118	-0.0248515043829659	01.08.2022	2.464	1.627
1.79769313486232e+308	0.00058438250918577 7	2.41272422665562	101347.2142485	01.08.2022	2.482	1.627	292.763079133012	-0.0238629381352702	01.08.2022	2.482	1.627
1.79769313486232e+308	0.00058431603958153 2	2.41275513532263	101346.734001094	01.08.2022	2.392	1.646	292.758373453175	-0.0245997756189017	01.08.2022	2.392	1.646
1.79769313486232e+308	0.00058435273482872 9	2.41273593577127	101346.83795333	01.08.2022	2.41	1.646	292.760881758459	-0.0243117235156357	01.08.2022	2.41	1.646
1.79769313486232e+308	0.00058422405196867 4	2.41280838155543	101346.903168839	01.08.2022	2.428	1.646	292.752142486901	-0.0251616790212724	01.08.2022	2.428	1.646
1.79769313486232e+308	0.00058428674521045 4	2.4127733524928	101346.918207357	01.08.2022	2.446	1.646	292.75640395271	-0.0247274085628905	01.08.2022	2.446	1.646
1.79769313486232e+308	0.00058428674521045 4	2.4127733524928	101346.918207357	01.08.2022	2.464	1.646	292.75640395271	-0.0247274085628905	01.08.2022	2.464	1.646
1.79769313486232e+308	0.00058429483780665 7	2.4127683935899	101346.886822694	01.08.2022	2.482	1.646	292.756971147821	-0.0238796101788196	01.08.2022	2.482	1.646
1.79769313486232e+308	0.00058714441499963 3	2.41112740404781	101343.414393268	01.08.2022	2.194	1.665	292.951105622876	-0.0198994521883251	01.08.2022	2.194	1.665
1.79769313486232e+308	0.00058534993084952 8	2.41214708018421	101343.808889573	01.08.2022	2.212	1.665	292.82782636526	-0.0205651404852356	01.08.2022	2.212	1.665
1.79769313486232e+308	0.00058486108250995 6	2.41242533203613	101344.208345932	01.08.2022	2.23	1.665	292.794505885867	-0.0212290063047477	01.08.2022	2.23	1.665
1.79769313486232e+308	0.00058479631828067 2	2.4124657092822	101344.593501104	01.08.2022	2.248	1.665	292.790216477033	-0.0207227690001116	01.08.2022	2.248	1.665
1.79769313486232e+308	0.00058477474080721 2	2.41248078781137	101344.959306828	01.08.2022	2.266	1.665	292.788886483577	-0.0203171322847922	01.08.2022	2.266	1.665

Figure 71: .csv table for case model, sliding door

E Run time

Simulation	PC	Mesh count	Simulation time	No. of processors	Runtime	Comment
Validation - sliding	Home PC	400,539	4s	2x8	8h 35min	
Validation - hinged	Home PC	673,221	4s	2x8	18h 10min	
Validation - double	Home PC	529,74	4s	2x8	4h 10min	
Model - sliding	FRAM	1,134,543	4s	3x32	6h 45min	
Model - hinged	FRAM	1,001,956	4s	3x32	6h 15min	
Model - double - 1st run	FRAM	1,340,047	4s	3x32	10h 55min	
Model - double - 2nd run	FRAM	1,340,047	4s	3x32	16h 00min	INCOMPLETE
Model - double - 3rd run	FRAM	1,340,047	4s	3x32	20h 00min	INCOMPLETE
Model - double - 4th run	Home PC	1,340,047	4s	2x8	25h 35min	

Figure 72: Run time for each model